OPTICAL AMPLIFIERS FOR 10 Gb/s WDM RECIRCULATING LOOP TESTBED

by

SRAVANTHI THOTAKURA

Presented to the Faculty of the Graduate School of

The University of Texas at Arlington in Partial Fulfillment

of the Requirements

for the Degree of

MASTER OF SCIENCE IN ELECTRICAL ENGINEERING

THE UNIVERSITY OF TEXAS AT ARLINGTON

August 2005

ACKNOWLEDGEMENTS

First and foremost I express my sincere gratitude to my advisor, Dr. Michael Vasilyev for his support, encouragement (appreciating even small improvements achieved), guidance and patience throughout my thesis. I got to learn a lot from him both in class and while working in lab with him. I want to use this opportunity to thank Dr. Nikolai Stelmakh for his emotional support and letting me be his teaching assistant especially for the lab. I would also like to thank Dr. Jung Chih Chiao and Dr. Weidong Zhou for serving on my committee and for their valuables suggestions and comments.

My heart felt thank to all my friends especially Kiran Bondalakunta for his encouragement and support through out my thesis, Harshavardhan and Venumadhav for helping me finish my document in time. I would also like to thank Surendra Gubbala for proof-reading my document and giving me helpful advice.

Finally I would like to thank my family especially my grandfather Mr. Ramamohan Rao Cherukuri who has been an inspiration to me through out my life. I would like to thank my parents and brother for their unconditional love and support. I would like to dedicate my work to my grandfather Mr. Ramamohan Rao Cherukuri.

July 22, 2005

ABSTRACT

OPTICAL AMPLIFIERS FOR 10 Gb/s RECIRCULATING-LOOP TESTBED

Publication No. _____

Sravanthi Thotakura, M.S.

The University of Texas at Arlington, 2005

Supervising Professor: Michael Vasilyev

This Master's thesis deals with building experimental setup for characterization of novel nonlinear optical devices for fiber communication.

The first part of the thesis deals with the description of the theoretical basis for operation of a particular type of such nonlinear optical devices, namely a parametric amplifier. Document includes deriving and solving the equations for parametric amplification in optical fiber when signal, idler and pump beams are linearly co-polarized. We consider both non-degenerate and degenerate pump cases for arbitrary phase mismatch.

In the second part of the thesis we present the design and experimental implementation of electrical interface between commercial ultra-long-haul-system

erbium-doped fiber amplifiers (EDFAs) and the laser diode drivers and thermo electric coolers used in our lab. We also describe the design and implementation of the electronic controller for EDFA's mid-stage variable optical attenuator that allows us to operate the EDFA at different input signal power levels. The interface and controller described in this thesis make it possible to use these EDFAs in a recirculating-loop testbed for characterization of novel nonlinear-optical devices.

TABLE OF CONTENTS

LIST OF ILLUSTRATIONS

Figure Page

LIST OF TABLES

Table Page

CHAPTER 1

INTRODUCTION

Tremendous progress in lightwave communications over the last decade has been closely related to the underlying advances in optical amplification technologies. Erbium-doped fiber amplifiers (EDFAs) have extended the reach of unregenerated transmission 10-fold and enabled processing of multiple wavelengths simultaneously, leading to the WDM revolution. The need for reduction of amplification noise below the noise-figure (NF) quantum limit was answered in late 1990s by progress the distributed Raman amplifiers which extended the link reach to several thousand kilometers, enabled higher bit rates and spectral efficiencies. By 2001–2002, Raman amplifier technology has become finally perfected by reaching the fundamental quantum limit of ideal distributed phase-insensitive amplifier (PIA) that provides the optimal trade-off between optical nonlinearity and spontaneous emission noise by balancing the local gain and loss coefficients at every point within the transmission span. Such performance, quantified by the product of overall span NF and nonlinear phase-shift, was shown to be within a fraction of a dB from its fundamental limit by the experiments using effective-area management in hybrid dispersion-managed fiber spans [1–3], and using the combination of bi-directional and second-order Raman pumping in a single-mode-fiber span [4]. Any further reduction in the span NF-nonlinearity product will require a novel revolutionary technology that is not bound by the quantum-

mechanical restrictions on distributed amplifier noise. Since the fiber capacity has a hard upper bound due, in part, to nonlinear coupling between the signals and noise [5], the search for this noise-mitigating technology is imperative for future systems.

Such promising technology is the phase-sensitive amplification. A lumped phase-sensitive amplifier (PSA) can amplify the signals without adding any noise, i.e. with NF of 0 dB, as opposed to the 3-dB NF limit of a lumped PIA (e.g. EDFA or Raman) [6]. Such a lumped noiseless fiber amplifier has been demonstrated, using nonlinear optical loop mirror [7, 8], based on pioneering works [9–11] on bulk-crystal PSAs.

Combining the properties of the distributed and phase-sensitive amplification would enable reaching the ultimate noise limit of linear amplification ("ideal distributed PSA limit") and give a revolutionary 3-dB signal-to-noise ratio advantage over the quantum limit of an ideal distributed PIA. When the thermal noise of Raman amplifier (additional 0.5 dB) and double Rayleigh backscattering noise (additional 0 dB to over 3 dB, depending on signal power) are taken into account, the actual advantage of the distributed PSA increases to 3.5–7 dB. However, because of the required distributed amplification in the transmission fiber span, the nonlinear optical interferometers, employed in the lumped case, cannot be used. The alternative approach involves parametric amplification in transmission fiber (for distributed amplification) or in highly-nonlinear fiber (for lumped amplification), where the parametric process is forced into a phase-sensitive regime by excitation of both signal and idler beams at the input [12].

In the first chapter of this thesis we show that parametric amplifier in optical fiber can indeed serve as a phase-sensitive amplifier. We derive and find the solution for the parametric amplification equations when the pumps, signal and idler are linearly co-polarized. We consider both degenerate and non-degenerate pump cases with arbitrary phase mismatch.

The second chapter deals with building the experimental infrastructure needed for characterization of parametric amplifiers and other novel nonlinear optical devices for optical communications. It describes the outline of the recirculating-loop testbed, as well as the design and implementation of

- an electrical interface connecting our lab's EDFAs to the laser diode drivers and thermo-electric coolers, and
- an electronic circuit controlling the variable optical attenuator that enables the EDFA to operate at various input signal power levels.

CHAPTER 2

THEORY OF PARAMETRIC AMPLIFICATION

2.1 Introduction

Parametric gain optical fibers can be used to make fiber-optic amplifiers and oscillators. Such devices have attracted considerable attention in the context of a phenomenon known as squeezing of quantum noise [7]. Parametric amplifiers may be used for signal amplification in fiber-optic communication systems. Parametric amplifiers have a moderately wide bandwidth (~1 THz) but the frequency shift can be as large as ~100 THz [13]. This permits considerable flexibility in the choice of a pump while, at the same time, the bandwidth is large enough for many applications.

When the two pumps have the same frequency, we have a degenerate pump case, and when they have different frequencies, we have a non-degenerate pump case. In this chapter, we will show that if only the signal is present at the input, then the amplifier operates in a phase-insensitive regime; if both signal and idler are present at the input, phase-sensitive amplification can be obtained.

We will start with Maxwell's equations and deal with the non-degenerate pump case in 2.2 and deal with the degenerate pump case in 2.3. Pumps, signal and idler are considered to be linearly co-polarized.

2.2 Non-Degenerate Pump Case

In the non-degenerate case, two photons at frequencies ω_1 and ω_2 are annihilated with simultaneous creation of two photons at frequencies ω_s and ω_i such that

$\omega_1 + \omega_2 = \omega_s + \omega_i$.

We define the electric field as

$\bar{e} = \overline{E} e^{-i\omega t} + c.c.$,

where $\overline{E}$ slowly varies with time.

Co-polarized four-wave mixing:

The pumps, signal and idler are linearly co-polarized:

E_y=0,

$$E_x = E_1 e^{-i\omega_1 t} + E_2 e^{-i\omega_2 t} + E_s e^{-i\omega_s t} + E_i e^{-i\omega_i t}$$

Nonlinear polarization of the medium has the form

$P_x = \varepsilon_0 \left(A + \frac{B}{2} \right) |E_x|^2 E_x$, where $A = 6\chi^{(3)}_{1122}$ and $B = 6\chi^{(3)}_{1221}$.

Let ω_1 and ω_2 be symmetric about ω:

$$\omega_1 = -\omega_2 \text{ and } \omega_s = -\omega_i$$

The condition for four-wave mixing is $\omega_s + \omega_i = \omega_1 + \omega_2$. We are interested in the polarization at frequency ω_s. The combinations that can produce ω_s are

$\omega_1 - \omega_1 + \omega_s$,

$\omega_2 - \omega_2 + \omega_s$,

$\omega_i - \omega_i + \omega_s$,

$\omega_s - \omega_s + \omega_s$,

$\omega_1 + \omega_2 - \omega_i$.

Therefore the polarization along ω_s is given by:

$$P_x(\omega_s) = \varepsilon_0\left(A + \frac{B}{2}\right)\left\{\left[|E_s|^2 + 2\left(|E_1|^2 + |E_2|^2 + |E_i|^2\right)\right]E_s + 2E_1E_2E_i^*\right\}.$$

Similarly, the polarization at frequency ω_i is given by the following equation (interchanging subscripts *s* and *i*):

$$P_x(\omega_i) = \varepsilon_0\left(A + \frac{B}{2}\right)\left\{\left[|E_i|^2 + 2\left(|E_1|^2 + |E_2|^2 + |E_s|^2\right)\right]E_i + 2E_1E_2E_s^*\right\}.$$

The combinations that can produce ω_1 are

$\omega_1 - \omega_1 + \omega_1$,

$\omega_2 - \omega_2 + \omega_1$,

$\omega_i - \omega_i + \omega_1$,

$\omega_s - \omega_s + \omega_1$,

$\omega_s + \omega_i - \omega_2$.

Therefore the polarization along ω_1 is given by:

$$P_x(\omega_1) = \varepsilon_0\left(A + \frac{B}{2}\right)\left\{\left[|E_1|^2 + 2\left(|E_2|^2 + |E_s|^2 + |E_i|^2\right)\right]E_1 + 2E_sE_iE_2^*\right\}.$$

Similarly, the polarization at frequency ω_2 is given by the following equation (interchanging subscripts 1 and 2):

$$P_x(\omega_2) = \varepsilon_0\left(A + \frac{B}{2}\right)\left\{\left[|E_2|^2 + 2\left(|E_1|^2 + |E_s|^2 + |E_i|^2\right)\right]E_2 + 2E_sE_iE_1^*\right\}.$$

Wave Equation:

$$\nabla^2 \bar{e} - \frac{1}{c^2}\frac{\partial^2 \bar{e}}{\partial t^2} = \mu_0 \frac{\partial^2 \bar{p}}{\partial t^2} = \mu_0 \frac{\partial^2}{\partial t^2}\left(\bar{p}^{\,l} + \bar{p}^{\,nl}\right), \tag{1}$$

$$\bar{e} = e^{-i\omega t}\sum_j \bar{E}_j e^{-i\omega_j t} + c.c., \tag{2}$$

$$\bar{p} = e^{-i\omega t}\sum_j \bar{P}_j e^{-i\omega_j t} + c.c., \tag{3}$$

$$\bar{P}_j = \bar{P}_j^{\,l} + \bar{P}_j^{\,nl}, \tag{4}$$

$$\bar{P}_j^{\,l} = \varepsilon_0 \chi(\omega + \omega_j)\bar{E}_j, \tag{5}$$

Substituting equations (2)–(5) in (1) gives

$$e^{-i\omega t}\sum_j \left\{\nabla^2 E_j + \frac{(\omega+\omega_j)^2}{c^2}E_j + \mu_0(\omega+\omega_j)^2[\varepsilon_0\chi(\omega+\omega_j)E_j + P_j^{nl}]\right\} e^{-i\omega_j t} + c.c. = 0,$$

$$\sum_j \left[\nabla^2 E_j + \frac{n_j^2(\omega+\omega_j)^2}{c^2}E_j + \mu_0(\omega+\omega_j)^2 P_j^{nl}\right] e^{-i(\omega+\omega_j)t} + c.c. = 0,$$

$$\nabla^2 E_j + \frac{n_j^2(\omega+\omega_j)^2}{c^2}E_j = -\mu_0(\omega+\omega_j)^2 P_j^{nl}\ , \tag{6}$$

where $\nabla^2 = \dfrac{\partial^2}{\partial x^2} + \dfrac{\partial^2}{\partial y^2} + \dfrac{\partial^2}{\partial z^2}$ and $n_j^2 = 1 + \chi(\omega+\omega_j)$.

We will look for the solution in the form of

$$E_j = F_j(x,y)A_j(z)e^{i\beta_j z}, \tag{7}$$

where $F_j(x,y)$ is the optical fiber mode profile and β_j is its propagation constant.

When there is no nonlinearity:

$A_j(z)$=const,

$$\nabla^2 E_j = \left(\nabla^2_{x,y} F_j\right) A_j e^{i\beta_j z} - \beta_j^2 F_j A_j e^{i\beta_j z} \ . \tag{8}$$

Substituting (7), (8) in (6) we get

$$\nabla^2_{x,y} F_j + \left[\frac{n_j^2(\omega+\omega_j)^2}{c^2} - \beta_j^2\right] F_j = 0 \ . \tag{9}$$

Nonlinear case:

$A_j(z)$ is slowly varying with *z*:

$$\nabla^2 E_j = A_j(z) e^{i\beta_j z} \nabla^2_{x,y} F_j + F_j\left(\frac{\partial^2 A_j}{\partial z^2} + 2i\beta_j \frac{\partial A_j}{\partial z} - \beta_j^2 A_j\right) e^{i\beta_j z} . \tag{10}$$

Slowly-Varying-Envelope Approximation: $\frac{\partial^2 A_j}{\partial z^2} << \beta_j \frac{\partial A_j}{\partial z}$, which means that $\frac{\partial A_j}{\partial z}$ changes over the length scale $\Lambda >> \lambda$. Substituting (10) and (7) in (6) and assuming $\frac{\partial^2 A_j}{\partial z^2} = 0$, we have:

$$e^{i\beta_j z}\left[A_j \nabla^2_{x,y} + 2i\beta_j \frac{\partial A_j}{\partial z} - \beta_j^2 A_j + \frac{n_j^2(\omega+\omega_j)^2}{c^2} A_j\right] F_j = -\mu_0(\omega+\omega_j)^2 P_j^{nl} , \tag{11}$$

Substituting result from (9) in (11), we obtain

$$\Rightarrow 2i\beta_j F_j \frac{\partial A_j}{\partial z} = -\mu_0\left(\omega+\omega_j\right)^2 P_j^{nl} e^{-i\beta_j z} \ .$$

Since $\omega_j << \omega$, we can assume $\omega + \omega_j \approx \omega$.

Therefore

$$2i\beta_s F_s \frac{\partial A_s}{\partial z} = -\mu_0 \omega^2 P_s^{nl} e^{-i\beta_s z} .$$

Substituting the result of $P_x(\omega_s)$ and (7) in the above, we have the following right-hand side:

$$= -\mu_0 \omega^2 \varepsilon_0 \left(A + \frac{B}{2} \right) \left\{ \left[|F_s|^2 |A_s|^2 + 2\left(|F_1|^2 |A_1|^2 + |F_2|^2 |A_2|^2 + |F_i|^2 |A_i|^2 \right) \right] F_s A_s \right.$$
$$\left. + 2F_1 F_2 F_i^* A_1 A_2 A_i^* e^{i(\beta_1 + \beta_2 - \beta_i - \beta_s)z} \right\}.$$

Let us multiply both sides with F_s^* and integrate over dxdy. Then

$$|A_j|^2 = W_j = \text{power [Watts]},$$

$$\int |F_j(x,y)|^2 \mathrm{d}x\mathrm{d}y = \frac{1}{2\varepsilon_0 n_j c} ,$$

$$[|F_j|^2] = \frac{1}{(2\varepsilon_0 n_j c) \times [\text{Area}]} - \text{dimension of } |F_j|^2 , \text{ and}$$

$$2i\beta_s \frac{\partial A_s}{\partial z} = -\frac{\omega^2}{c^2} \left(A + \frac{B}{2} \right) \frac{1}{\int |F_s|^2 \mathrm{d}x\mathrm{d}y} \left\{ \left[|A_s|^2 + \int |F_s|^4 \mathrm{d}x\mathrm{d}y + \right. \right.$$
$$\left. + 2\left(|A_1|^2 \int |F_1|^2 |F_s|^2 \mathrm{d}x\mathrm{d}y + |A_2|^2 \int |F_2|^2 |F_s|^2 \mathrm{d}x\mathrm{d}y + |A_i|^2 \int |F_i|^2 |F_s|^2 \mathrm{d}x\mathrm{d}y \right) \right] A_s \qquad (12)$$
$$\left. + 2A_1 A_2 A_i^* \int F_1 F_2 F_i^* F_s^* \mathrm{d}x\mathrm{d}y e^{i\Delta\beta z} \right\}.$$

Here $\Delta\beta = \beta_1 + \beta_2 - \beta_s - \beta_i$ is linear phase mismatch,

$$\frac{\int F_m F_n F_k^* F_l^* \mathrm{d}x\mathrm{d}y}{\int |F_s|^2 \mathrm{d}x\mathrm{d}y} \approx \frac{\int |F_s|^4 \mathrm{d}x\mathrm{d}y}{\int |F_s|^2 \mathrm{d}x\mathrm{d}y} = \frac{1}{2\varepsilon_0 n_s c A_{\text{eff}}} , \qquad (13)$$

and A_{eff} is the effective area of the fiber. Substituting equation (13) in (12) and solving for $\frac{\partial A_s}{\partial z}$, we have

$$\frac{\partial A_s}{\partial z} = \frac{i\omega}{2n_s c}\frac{\left(A+\frac{B}{2}\right)}{2\varepsilon_0 n_s c A_{\text{eff}}}\left\{\left[|A_s|^2 + 2\left(|A_1|^2 + |A_2|^2 + |A_i|^2\right)\right]A_s + 2A_1A_2A_i^* e^{i\Delta\beta z}\right\} =$$

$$= \frac{in_2^l\omega}{cA_{\text{eff}}}\left\{\left[|A_s|^2 + 2\left(|A_1|^2 + |A_2|^2 + |A_i|^2\right)\right]A_s + 2A_1A_2A_i^* e^{i\Delta\beta z}\right\} \ ,$$

where $n_2^l = \frac{A + B/2}{4\varepsilon_0 n_s^2 c}$. Then

$$\frac{\partial A_s}{\partial z} = i\gamma\left\{\left[|A_s|^2 + 2\left(|A_1|^2 + |A_2|^2 + |A_i|^2\right)\right]A_s + 2A_1A_2A_i^* e^{i\Delta\beta z}\right\} \ , \tag{14}$$

where γ is nonlinear constant given by $\gamma = \frac{n_2^l\omega}{cA_{\text{eff}}}$.

Similarly,

$$\frac{\partial A_i}{\partial z} = i\gamma\left\{\left[|A_i|^2 + 2\left(|A_1|^2 + |A_2|^2 + |A_s|^2\right)\right]A_i + 2A_1A_2A_s^* e^{i\Delta\beta z}\right\} \ , \tag{15}$$

$$\frac{\partial A_1}{\partial z} = i\gamma\left\{\left[|A_1|^2 + 2\left(|A_2|^2 + |A_s|^2 + |A_i|^2\right)\right]A_1 + 2A_sA_iA_2^* e^{-i\Delta\beta z}\right\} \ , \tag{16}$$

$$\frac{\partial A_2}{\partial z} = i\gamma\left\{\left[|A_2|^2 + 2\left(|A_1|^2 + |A_s|^2 + |A_i|^2\right)\right]A_2 + 2A_sA_iA_1^* e^{-i\Delta\beta z}\right\} \ . \tag{17}$$

Undepleted pump approximation:

$$A_{s,i} << A_{1,2}\,, \tag{18}$$

hence we can neglect the change in pump power due to parametric interaction. Substituting the result from (18) in (16) and (17), we have

$$\frac{\partial A_1}{\partial z} = i\gamma\left(|A_1|^2 + 2|A_2|^2\right)A_1 \ , \tag{19}$$

$$\frac{\partial A_2}{\partial z} = i\gamma\left(|A_2|^2 + 2|A_1|^2\right)A_2\,. \tag{20}$$

We have $\left|A_{1,2}(z)\right|^2 = W_{1,2} = \text{const}$. Substituting this value in (19), (20), (14) and (15), we have

$$\frac{\partial A_1}{\partial z} = i\gamma(W_1 + 2W_2)A_1 \ , \tag{21}$$

$$\Rightarrow A_1(z) = A_1(0)e^{i\gamma(W_1+2W_2)z} , \tag{22}$$

$$\frac{\partial A_2}{\partial z} = i\gamma(W_2 + 2W_1)A_2 \ , \tag{23}$$

$$\Rightarrow A_2(z) = A_2(0)e^{i\gamma(W_2+2W_1)z} \ , \tag{24}$$

and the signal and idler equations

$$\frac{\partial A_s}{\partial z} = i\gamma\left[(2W_1 + 2W_2)A_s + 2A_1A_2A_i^*e^{i\Delta\beta z}\right] , \tag{25}$$

$$\frac{\partial A_i}{\partial z} = i\gamma\left[(2W_1 + 2W_2)A_i + 2A_1A_2A_s^*e^{i\Delta\beta z}\right] . \tag{26}$$

Let $A_s = B_s(z)e^{2i\gamma(W_1+W_2)z}$, (27)

and $A_i = B_i(z)e^{2i\gamma(W_1+W_2)z}$. (28)

Then

$$\frac{\partial B_s}{\partial z} = 2i\gamma\sqrt{W_1W_2}\,B_i^*e^{i[\Delta\beta-\gamma(W_1+W_2)]z} \ , \tag{29}$$

$$\frac{\partial B_i}{\partial z} = 2i\gamma\sqrt{W_1W_2}\,B_s^*e^{i[\Delta\beta-\gamma(W_1+W_2)]z} \ . \tag{30}$$

Here we assume $A_{1,2}(0) = \sqrt{W_{1,2}}$, i.e. the initial pump phases are zero.

Let $B_s = B_s'e^{\frac{i[\Delta\beta-\gamma(W_1+W_2)]z}{2}}$ (31)

and $B_i = B_i' e^{\frac{i[\Delta\beta - \gamma(W_1+W_2)]z}{2}}$. (32)

Then

$$\frac{\partial B_s'}{\partial z} = -\frac{i}{2}\left[\Delta\beta - \gamma\left(W_1 + W_2\right)\right]B_s' + 2i\gamma\sqrt{W_1W_2}\,B_i'^{*}, \tag{33}$$

$$\frac{\partial B_i'^{*}}{\partial z} = -2i\gamma\sqrt{W_1W_2}\,B_s' + \frac{i}{2}\left[\Delta\beta - \gamma\left(W_1 + W_2\right)\right]B_i'^{*} \ . \tag{34}$$

Equations (33), (34) can be represented in matrix form as

$$\frac{\mathrm{d}}{\mathrm{d}z}\begin{bmatrix} B_s' \\ B_i'^{*} \end{bmatrix} = \begin{bmatrix} \dfrac{-i\left[\Delta\beta - \gamma(W_1+W_2)\right]}{2} & 2i\gamma\sqrt{W_1W_2} \\ -2i\gamma\sqrt{W_1W_2} & \dfrac{i\left[\Delta\beta - \gamma(W_1+W_2)\right]}{2} \end{bmatrix}\begin{bmatrix} B_s' \\ B_i'^{*} \end{bmatrix}. \tag{35}$$

Let $\mathrm{M} = \begin{bmatrix} \dfrac{-i\left[\Delta\beta - \gamma(W_1+W_2)\right]}{2} & 2i\gamma\sqrt{W_1W_2} \\ -2i\gamma\sqrt{W_1W_2} & \dfrac{i\left[\Delta\beta - \gamma(W_1+W_2)\right]}{2} \end{bmatrix}$.

To find the eigenvalues of Eq. (35), we need to solve the following algebraic equation:

$\det\left(\mathrm{M} - \lambda\mathrm{I}\right) = 0$, or

$$\begin{vmatrix} -\dfrac{i[\Delta\beta - \gamma(W_1+W_2)]}{2} - \lambda & 2i\gamma\sqrt{W_1W_2} \\ -2i\gamma\sqrt{W_1W_2} & \dfrac{i[\Delta\beta - \gamma(W_1+W_2)]}{2} - \lambda \end{vmatrix} = 0,$$

$$\Rightarrow \frac{\left[\Delta\beta - \gamma(W_1+W_2)\right]^2}{4} + \lambda^2 - 4\gamma^2 W_1W_2 = 0 \ . \tag{36}$$

Solving (36) we have

$$\lambda_{1,2} = \pm\sqrt{4\gamma^2 W_1W_2 - \frac{\left[\Delta\beta - \gamma(W_1+W_2)\right]^2}{4}} \ .$$

For λ_1 and λ_2 to be real, we need $4\gamma^2 W_1 W_2 \geq \frac{\left[\Delta\beta - \gamma(W_1 + W_2)\right]^2}{4} = \frac{\kappa^2}{4}$,

where $\kappa = \Delta\beta - \gamma(W_1 + W_2)$ is the net phase mismatch (linear plus nonlinear). Substituting (31) in (27), we have

$$A_s(z) = B_s'(z) e^{\frac{i\Delta\beta z}{2}} e^{\frac{3i\gamma(W_1+W_2)z}{2}} , \tag{37}$$

The solution of Eq. (35) has the form of

$$B_s'(z) = D_1 \cosh\lambda z + D_2 \sinh\lambda z , \tag{38}$$

$\lambda = |\lambda_{1,2}|$.

No phase mismatch: $\kappa = 0$,

i.e. $\gamma(W_1 + W_2) = \Delta\beta$ and $\lambda = 2\gamma\sqrt{W_1 W_2}$.

$B_s'(z) = A_s(0)\cosh\lambda z + A_i^*(0)\sinh\lambda z$,

$B_i'(z) = A_i(0)\cosh\lambda z + A_s^*(0)\sinh\lambda z$.

Therefore the equations for signal and idler are given by:

$$A_s(z) = \left[A_s(0)\cosh\lambda z + A_i^*(0)\sinh\lambda z\right] e^{\frac{i\Delta\beta z}{2}} e^{\frac{3i\gamma(W_1+W_2)z}{2}} , \tag{39}$$

$$A_i(z) = \left[A_i(0)\cosh\lambda z + A_s^*(0)\sinh\lambda z\right] e^{\frac{i\Delta\beta z}{2}} e^{\frac{3i\gamma(W_1+W_2)z}{2}} . \tag{40}$$

If input $A_s(0)=A_i(0)=|A_0|e^{i\theta}$, then the parametric gain $G = \left|\frac{A_s(z)}{A_s(0)}\right|^2 =$

$= \left|e^{i\theta}\cosh\lambda z + e^{-i\theta}\sinh\lambda z\right|^2$ depends on the input signal phase θ, i.e. G is phase

sensitive. When θ = 0, we have maximum phase-sensitive amplification, i.e. $G = e^{2\lambda z}$. If $\theta = \frac{\pi}{2}$, then we have phase-sensitive deamplification: $G = e^{-2\lambda z}$.

When there is phase mismatch: $\kappa \neq 0$.

$B_s'(z) = D_1 \cosh \lambda z + D_2 \sinh \lambda z$.

If we put $z = 0$ in the above equation, we have

$D_1 = B_s'(0)$.

Substituting $z = 0$ in (31), we have

$D_1 = B_s(0)$.

Substituting $z = 0$ in (27), we have

$$D_1 = A_s(0). \tag{41}$$

First derivative of (38) is given by

$$\frac{\partial B_s'}{\partial z} = D_1 \lambda \sinh \lambda z + D_2 \lambda \cosh \lambda z \ . \tag{42}$$

Finding the derivative of (37) at $z = 0$ and substituting the value of $B_s'(0)$ from (38), we have

$$\left.\frac{\partial A_s}{\partial z}\right|_{z=0} = D_2 \lambda + \frac{i[\Delta\beta + 3\gamma(W_1 + W_2)]}{2} A_s(0) \ . \tag{43}$$

Substituting the value of $z = 0$ in (25) and using $A_1 A_2 = \sqrt{W_1 W_2}$, we have,

$$\left.\frac{\partial A_s}{\partial z}\right|_{z=0} = 2i\gamma\sqrt{W_1 W_2}\, A_i^*(0) + 2i\gamma(W_1 + W_2) A_s(0) \ . \tag{45}$$

From (43) and (45) we find that D_2 is given by

$$D_2 = \frac{2i\gamma\sqrt{W_1 W_2}\, A_i^*(0) - \frac{i\left[\Delta\beta - \gamma(W_1 + W_2)\right]}{2} A_s(0)}{\lambda} \quad . \tag{46}$$

Substituting the results from (41) and (46) in (38) and, in turn, substituting in (37), we obtain the solution for the signal and idler as

$$A_s(z) = \left\{ A_s(0)\cosh\lambda z + \frac{2i\gamma\sqrt{W_1 W_2}\, A_i^*(0) - \frac{i\left[\Delta\beta - \gamma(W_1 + W_2)\right]}{2} A_s(0)}{\lambda} \sinh\lambda z \right\} e^{\frac{i\Delta\beta z}{2}} e^{\frac{3i\gamma(W_1+W_2)z}{2}} =$$

$$= A_s(0)\left\{ \cosh\lambda z - \frac{i\left[\Delta\beta - \gamma(W_1 + W_2)\right]}{2\lambda} \sinh\lambda z \right\} e^{\frac{i\Delta\beta z}{2}} e^{\frac{3i\gamma(W_1+W_2)z}{2}} +$$

$$+ A_i^*(0) \frac{2i\gamma\sqrt{W_1 W_2}}{\lambda} \sinh\lambda z \; e^{\frac{i\Delta\beta z}{2}} e^{\frac{3i\gamma(W_1+W_2)z}{2}} \quad ,$$

$$A_i(z) = \left\{ A_i(0)\cosh\lambda z + \frac{2i\gamma\sqrt{W_1 W_2}\, A_s^*(0) - \frac{i\left[\Delta\beta - \gamma(W_1 + W_2)\right]}{2} A_i(0)}{\lambda} \sinh\lambda z \right\} e^{\frac{i\Delta\beta z}{2}} e^{\frac{3i\gamma(W_1+W_2)z}{2}} =$$

$$= A_s^*(0) \frac{2i\gamma\sqrt{W_1 W_2}}{\lambda} \sinh\lambda z \; e^{\frac{i\Delta\beta z}{2}} e^{\frac{3i\gamma(W_1+W_2)z}{2}} +$$

$$+ A_i(0)\left\{ \cosh\lambda z - \frac{i\left[\Delta\beta - \gamma(W_1 + W_2)\right]}{2\lambda} \sinh\lambda z \right\} e^{\frac{i\Delta\beta z}{2}} e^{\frac{3i\gamma(W_1+W_2)z}{2}} \quad .$$

Same phase sensitive behavior is also observed here. Phase of idler $A_i^*(0)$ term is given by $\frac{\pi}{2} - \theta$ and phase of $A_s(0)$ is given by $\theta - \tan^{-1}\left[\frac{\Delta\beta - \gamma(W_1 + W_2)}{2\lambda}\tanh\lambda z\right]$.

We have maximum amplification when both the phases are equal i.e. $\theta = \theta_{max}$

$= -\frac{\pi}{4} - \frac{1}{2}\tan^{-1}\left[\frac{\Delta\beta - \gamma(W_1 + W_2)}{2\lambda}\tanh\lambda z\right]$. We have phase-sensitive deamplification at

$\theta = \theta_{max} + \frac{\pi}{2}$.

2.3 Degenerate Case

Four-wave mixing in degenerate pump case ($\omega_1 = \omega_2$) transfers the energy from strong pump wave to two waves up-shifted and down-shifted in frequency from the pump frequency by an amount $\Omega_s = \omega_1 - \omega_s = \omega_i - \omega_1$.

Our electric field definition is

$\bar{e} = \bar{E}e^{-i\omega t} + c.c.$

Co-polarized four-wave mixing:

The pumps, signal and idler are linearly co-polarized.

$E_y = 0$,

$E_x = E_1 e^{-i\omega_1 t} + E_s e^{-i\omega_s t} + E_i e^{-i\omega_i t}$.

Nonlinear polarization of the medium has the form

$P_x = \varepsilon_0\left(A + \frac{B}{2}\right)|E_x|^2 E_x$, where $A = 6\chi^{(3)}_{1122}$ and $B = 6\chi^{(3)}_{1221}$.

The condition for four-wave mixing is $2\omega_1 = \omega_i + \omega_s$. We are interested in the polarization at frequency ω_s. The combinations that can produce ω_s are

$\omega_1 - \omega_1 + \omega_s$,

$\omega_i - \omega_i + \omega_s$,

$\omega_s - \omega_s + \omega_s$,

$\omega_1 + \omega_1 - \omega_i$.

Therefore the polarization along ω_s is given by

$$P_x(\omega_s) = \varepsilon_0\left(A + \frac{B}{2}\right)\left\{\left[|E_s|^2 + 2\left(|E_1|^2 + |E_i|^2\right)\right]E_s + E_1{}^2 E_i^*\right\}.$$

Similarly, the polarization at frequency ω_i is given by the following equation:

$$P_x(\omega_i) = \varepsilon_0\left(A + \frac{B}{2}\right)\left\{\left[|E_i|^2 + 2\left(|E_1|^2 + |E_s|^2\right)\right]E_i + E_1{}^2 E_s^*\right\}.$$

The combinations that can produce ω_1 are

$\omega_1 - \omega_1 + \omega_1$,

$\omega_i - \omega_i + \omega_1$,

$\omega_s - \omega_s + \omega_1$,

$\omega_s + \omega_i - \omega_1$.

Therefore the polarization along ω_1 is given by

$$P_x(\omega_1) = \varepsilon_0\left(A + \frac{B}{2}\right)\left\{\left[|E_1|^2 + 2\left(|E_i|^2 + |E_s|^2\right)\right]E_1 + 2E_s E_i E_1^*\right\}.$$

Wave Equation:

$$\nabla^2\bar{e} - \frac{1}{c^2}\frac{\partial^2\bar{e}}{\partial t^2} = \mu_0\frac{\partial^2\bar{p}}{\partial t^2} = \mu_0\frac{\partial^2}{\partial t^2}\left(\bar{p}^l + \bar{p}^{nl}\right), \tag{47}$$

$$\bar{e} = e^{-i\omega t}\sum_j \bar{E}_j e^{-i\omega_j t} + c.c. , \tag{48}$$

$$\bar{p} = e^{-i\omega t}\sum_j \bar{P}_j e^{-i\omega_j t} + c.c. , \tag{49}$$

$$\bar{P}_j = \bar{P}_j^l + \bar{P}_j^{nl} , \tag{50}$$

$$\overline{P}_j^l = \varepsilon_0 \chi(\omega+\omega_j)\overline{E}_j \ . \tag{51}$$

Substituting Eqs. (48)–(51) in (47) gives

$$e^{-i\omega t}\sum_j \left\{ \nabla^2 E_j + \frac{(\omega+\omega_j)^2}{c^2} E_j + \mu_0(\omega+\omega_j)^2[\varepsilon_0\chi(\omega+\omega_j)E_j + P_j^{nl}] \right\} e^{-i\omega_j t} + c.c. = 0 ,$$

$$\sum_j \left[\nabla^2 E_j + \frac{n_j^2(\omega+\omega_j)^2}{c^2} E_j + \mu_0(\omega+\omega_j)^2 P_j^{nl} \right] e^{-i(\omega+\omega_j)t} + c.c. = 0 ,$$

$$\nabla^2 E_j + \frac{n_j^2(\omega+\omega_j)^2}{c^2} E_j = -\mu_0(\omega+\omega_j)^2 P_j^{nl} \ , \tag{52}$$

where $\nabla^2 = \frac{\partial^2}{\partial x^2} + \frac{\partial^2}{\partial y^2} + \frac{\partial^2}{\partial z^2}$ and $n_j^2 = 1 + \chi(\omega+\omega_j)$.

We will look for the solution in the form of

$$E_j = F_j(x,y)A_j(z)e^{i\beta_j z} \ , \tag{53}$$

where $F_j(x,y)$ is the optical fiber mode profile and β_j is its propagation constant.

When there is no nonlinearity:

$A_j(z)$=const,

$$\nabla^2 E_j = \left(\nabla_{x,y}^2 F_j\right) A_j e^{i\beta_j z} - \beta_j^2 F_j A_j e^{i\beta_j z} \ , \tag{54}$$

Substituting (53) and (54) in (52), we get

$$\nabla_{x,y}^2 F_j + \left[\frac{n_j^2(\omega+\omega_j)^2}{c^2} - \beta_j^2 \right] F_j = 0 \ . \tag{55}$$

Nonlinear case:

$A_j(z)$ is slowly varying with z:

$$\nabla^2 E_j = A_j(z)e^{i\beta_j z}\nabla_{x,y}^2 F_j + F_j\left(\frac{\partial^2 A_j}{\partial z^2} + 2i\beta_j \frac{\partial A_j}{\partial z} - \beta_j^2 A_j\right)e^{i\beta_j z} \ , \tag{56}$$

***Slowly Varying Envelope Approximation*:** $\frac{\partial^2 A_j}{\partial z^2} << \beta_j \frac{\partial A_j}{\partial z}$, which means that $\frac{\partial A_j}{\partial z}$ changes over the length scale $\Lambda >> \lambda$.

Substituting (56) and (53) in (52) and assuming $\frac{\partial^2 A_j}{\partial z^2} = 0$, we have:

$$e^{i\beta_j z}\left[A_j\nabla_{x,y}^2 + 2i\beta_j \frac{\partial A_j}{\partial z} - \beta_j^2 A_j + \frac{n_j^2(\omega+\omega_j)^2}{c^2}A_j\right]F_j = -\mu_0(\omega+\omega_j)^2 P_j^{nl} \ , \tag{57}$$

Substituting the result from (55) in (57), we obtain

$$2i\beta_j F_j \frac{\partial A_j}{\partial z} = -\mu_0\left(\omega+\omega_j\right)^2 P_j^{nl} e^{-i\beta_j z} \quad .$$

Since $\omega_j << \omega$, we can assume $\omega + \omega_j \approx \omega$. Therefore

$$2i\beta_s F_s \frac{\partial A_s}{\partial z} = -\mu_0\omega^2 P_s^{nl} e^{-i\beta_s z}$$

Substituting the result of $P_x(\omega_s)$ and (53) in the above we have the following right hand side:

$$= -\mu_0\omega^2\varepsilon_0\left(A + \frac{B}{2}\right)\left\{\left[|F_s|^2|A_s|^2 + 2\left(|F_1|^2|A_1|^2 + |F_i|^2|A_i|^2\right)\right]F_s A_s + F_1^2 F_i^* A_1^2 A_i^* e^{i(2\beta_1-\beta_s-\beta_i)z}\right\}$$

Let us multiply both sides with F_s^* and integrate over d*x*d*y*. Then

$$\left|A_j\right|^2 = W_j = \text{power [Watts]} \ , \tag{58}$$

$$\int \left|F_j(x,y)\right|^2 \mathrm{d}x\mathrm{d}y = \frac{1}{2\varepsilon_0 n_j c},$$

$$[|F_j|^2] = \frac{1}{(2\varepsilon_0 n_j c)\times[\text{Area}]} \text{ – dimension of } |F_j|^2, \text{ and}$$

$$2i\beta_s \frac{\partial A_s}{\partial z} = -\frac{\omega^2}{c^2}\left(A + \frac{B}{2}\right)\frac{1}{\int |F_s|^2 \mathrm{d}x\mathrm{d}y}\left\{\left[|A_s|^2 \int |F_s|^2 \mathrm{d}x\mathrm{d}y + 2\left(|A_s|^2 \int |F_1|^2 |F_s|^2 \mathrm{d}x\mathrm{d}y + \right.\right.\right. \\ \left.\left.\left. + |A_i|^2 \int |F_i|^2 |F_s|^2 \mathrm{d}x\mathrm{d}y\right)\right]A_S + A_1^2 A_i^* \int F_1^2 F_i^* F_s^* \mathrm{d}x\mathrm{d}y e^{i\Delta\beta z}\right\}. \quad (59)$$

Here $\Delta\beta = 2\beta_1 - \beta_s - \beta_i$ is linear phase mismatch,

$$\frac{\int F_m F_n F_k^* F_l^* \mathrm{d}x\mathrm{d}y}{\int |F_s|^2 \mathrm{d}x\mathrm{d}y} \approx \frac{\int |F_s|^4 \mathrm{d}x\mathrm{d}y}{\int |F_s|^2 \mathrm{d}x\mathrm{d}y} = \frac{1}{2\varepsilon_0 n_s c A_{\text{eff}}}, \quad (60)$$

and A_{eff} is the effective area of the fiber.

Substituting (60) in (59) and solving for $\frac{\partial A_s}{\partial z}$, we have

$$\frac{\partial A_s}{\partial z} = \frac{i\omega}{2n_s c}\frac{\left(A + \frac{B}{2}\right)}{2\varepsilon_0 n_s c A_{\text{eff}}}\left\{\left[|A_s|^2 + 2\left(|A_1|^2 + |A_i|^2\right)\right]A_s + A_1^2 A_i^* e^{i\Delta\beta z}\right\}$$

$$= \frac{i n_2^l \omega}{c A_{\text{eff}}}\left\{\left[|A_s|^2 + 2\left(|A_1|^2 + |A_i|^2\right)\right]A_s + A_1^2 A_i^* e^{i\Delta\beta z}\right\},$$

where $n_2^l = \frac{A + B/2}{4\varepsilon_0 n_s^2 c}$. Then

$$\frac{\partial A_s}{\partial z} = i\gamma\left\{\left[|A_s|^2 + 2\left(|A_1|^2 + |A_i|^2\right)\right]A_s + A_1^2 A_i^* e^{i\Delta\beta z}\right\}, \quad (61)$$

where γ is nonlinear constant and is given by $\gamma = \frac{n_2^l \omega}{c A_{\text{eff}}}$. Similarly,

$$\frac{\partial A_i}{\partial z} = i\gamma\left\{\left[\left|A_i\right|^2 + 2\left(\left|A_1\right|^2 + \left|A_s\right|^2\right)\right]A_i + A_1^2 A_s^* e^{i\Delta\beta z}\right\}, \tag{62}$$

$$\frac{\partial A_1}{\partial z} = i\gamma\left\{\left[\left|A_1\right|^2 + 2\left(\left|A_s\right|^2 + \left|A_i\right|^2\right)\right]A_1 + 2A_s A_i A_1^* e^{-i\Delta\beta z}\right\}. \tag{63}$$

Note the absence of the factor of 2 in front of the four-wave mixing term $A_1^2 A_{s,i}^*$ in Eqs. (61) and (62) in contrast to the non-degenerate pump case of Eqs. (14), (15).

Undepleted pump approximation:

$$A_{s,i} << A_{1,2}, \tag{64}$$

hence we can neglect the change in pump power due to parametric interaction. Substituting the result from (64) in (63), we have

$$\frac{\partial A_1}{\partial z} = i\gamma \mid A_1 \mid^2 A_1 . \tag{65}$$

Substituting (58) in (65), (61) and (62), we have

$$\frac{\partial A_1}{\partial z} = i\gamma W_1 A_1 , \tag{66}$$

$$\Rightarrow A_1(z) = A_1(0)e^{i\gamma W_1 z} , \tag{67}$$

and the signal and idler equations

$$\frac{\partial A_s}{\partial z} = i\gamma\left(2W_1 A_s + A_1^2 A_i^* e^{i\Delta\beta z}\right), \tag{68}$$

$$\frac{\partial A_i}{\partial z} = i\gamma\left(2W A_i + A_1^2 A_s^* e^{i\Delta\beta z}{}_1\right) . \tag{69}$$

Let $A_s = B_s(z)e^{2i\gamma W_1 z}$, (70)

and $A_i = B_i(z)e^{2i\gamma W_1 z}$. (71)

Then

$$\frac{\partial B_s}{\partial z} = i\gamma W_1 B_i^* e^{i[\Delta\beta - 2\gamma W_1]z} \quad , \tag{72}$$

$$\frac{\partial B_i}{\partial z} = i\gamma W_1 B_s^* e^{i[\Delta\beta - 2\gamma W_1]z} \quad . \tag{73}$$

Here, we have assumed $A_{1,2}(0) = \sqrt{W_1}$, i.e. the initial pump phase is zero.

$$\text{Let } B_s = B_s' e^{\frac{i(\Delta\beta - 2\gamma W_1)z}{2}} \quad , \tag{74}$$

$$\text{and } B_i = B_i' e^{\frac{i(\Delta\beta - 2\gamma W_1)z}{2}} \quad . \tag{75}$$

Then

$$\frac{\partial B_s'}{\partial z} = -\frac{i}{2}\left[\Delta\beta - 2\gamma W_1\right]B_s' + i\gamma W_1 B_i'^* \, , \tag{76}$$

$$\frac{\partial B_i'^*}{\partial z} = -i\gamma W_1 B_s' + \frac{i}{2}\left[\Delta\beta - 2\gamma W_1\right]B_i'^* \quad . \tag{77}$$

Equations (76) and (77) can be represented in matrix form as

$$\frac{\mathrm{d}}{\mathrm{d}z}\begin{bmatrix} B_s' \\ B_i'^* \end{bmatrix} = \begin{bmatrix} \dfrac{-i\left[\Delta\beta - 2\gamma W_1\right]}{2} & i\gamma W_1 \\ -i\gamma W_1 & \dfrac{i\left[\Delta\beta - 2\gamma W_1\right]}{2} \end{bmatrix}\begin{bmatrix} B_s' \\ B_i'^* \end{bmatrix} \, . \tag{78}$$

$$\text{Let } \mathrm{M} = \begin{bmatrix} \dfrac{-i\left[\Delta\beta - 2\gamma W_1\right]}{2} & i\gamma W_1 \\ -i\gamma W_1 & \dfrac{i\left[\Delta\beta - 2\gamma W_1\right]}{2} \end{bmatrix} .$$

To find the eigenvalues of Eq. (78), we need to solve the following algebraic equation:

$\det(\mathrm{M} - \lambda \mathrm{I}) = 0$, or

$$\begin{vmatrix} \frac{-i[\Delta\beta - 2\gamma W_1]}{2} - \lambda & i\gamma W_1 \\ -i\gamma W_1 & \frac{i[\Delta\beta - 2\gamma W_1]}{2} - \lambda \end{vmatrix} = 0,$$

$$\Rightarrow \frac{(\Delta\beta - 2\gamma W_1)^2}{4} + \lambda^2 - \gamma^2 W_1^2 = 0 \ . \tag{79}$$

Solving (79) we have

$$\lambda_{1,2} = \pm\sqrt{\gamma^2 W_1^2 - \frac{(\Delta\beta - 2\gamma W_1)^2}{4}} = \sqrt{\frac{(4\gamma W_1 - \Delta\beta)\Delta\beta}{4}} \ .$$

For λ_1 and λ_2 to be real, we need $\gamma^2 W_1^2 > \frac{(\Delta\beta - 2\gamma W_1)^2}{4} = \frac{\kappa^2}{4}$, where $\kappa = \Delta\beta - 2\gamma W_1$ is the net phase mismatch (linear plus nonlinear). This condition is satisfied for $\gamma W_1 > \Delta\beta/4$, $\Delta\beta > 0$. Substituting (74) in (70), and (75) in (71), we have

$$A_s(z) = B_s'(z) e^{\frac{i\Delta\beta z}{2}} e^{i\gamma W_1 z} \ , \tag{80}$$

$$A_i(z) = B_i'(z) e^{\frac{i\Delta\beta z}{2}} e^{i\gamma W_1 z} \ . \tag{81}$$

The solution for Eq. (78) has the form of

$$B_s'(z) = D_1 \cosh\lambda z + D_2 \sinh\lambda z \ , \tag{82}$$

$\lambda = |\lambda_{1,2}|$.

No phase mismatch: $\kappa = 0$,

i.e. $\gamma W_1 = \frac{\Delta\beta}{2}$ and $\lambda = \gamma W_1$.

$$B_s'(z) = A_s(0)\cosh\lambda z + A_i^*(0)\sinh\lambda z$$

$$B_i'(z) = A_i(0)\cosh\lambda z + A_s^*(0)\sinh\lambda z$$

Therefore the equations for signal and idler are given by:

$$A_s(z) = \left[A_s(0)\cosh\lambda z + A_i^*(0)\sinh\lambda z\right] e^{\frac{i\Delta\beta z}{2}} e^{i\gamma W_1 z} \ , \tag{83}$$

$$A_i(z) = \left[A_i(0)\cosh\lambda z + A_s^*(0)\sinh\lambda z\right] e^{\frac{i\Delta\beta z}{2}} e^{i\gamma W_1 z} \ . \tag{84}$$

If input $A_s(0)=A_i(0)=|A_0|e^{i\theta}$, then the parametric gain $G = \left|\frac{A_s(z)}{A_s(0)}\right|^2 =$

$= \left|e^{i\theta}\cosh\lambda z + e^{-i\theta}\sinh\lambda z\right|^2$ depends on the input signal phase θ, i.e. G is phase sensitive. When θ = 0, we have maximum phase-sensitive amplification, i.e. $G = e^{2\lambda z}$. If $\theta = \frac{\pi}{2}$, then we have phase-sensitive deamplification: $G = e^{-2\lambda z}$.

When there is phase mismatch: $\kappa \neq 0$.

$B_s'(z) = D_1\cosh\lambda z + D_2\sinh\lambda z$.

If we put $z = 0$ in the above equation, we have

$D_1 = B_s'(0)$.

Substituting $z = 0$ in (74) we have

$D_1 = B_s(0)$.

Substituting $z = 0$ in (70) we have

$$D_1 = A_s(0). \tag{85}$$

First derivative of (82) is given by

$$\frac{\partial B_s'}{\partial z} = D_1\lambda\sinh\lambda z + D_2\lambda\cosh\lambda z \ , \tag{86}$$

Finding the first derivative of (80) at $z = 0$ and substituting the value of $B_s'(0)$ from (82), we have

$$\left.\frac{\partial A_s}{\partial z}\right|_{z=0} = D_2\lambda + \frac{i(\Delta\beta + 2\gamma W_1)}{2} A_s(0). \tag{87}$$

Substituting the value of $z = 0$ in (61) and using $A_1^2 = W_1$, we have

$$\left.\frac{\partial A_s}{\partial z}\right|_{z=0} = i\gamma W_1 A_i^*(0) + 2i\gamma W_1 A_s(0). \tag{88}$$

From (87) and (88) we find that D_2 is given by

$$D_2 = \frac{i\gamma W_1 A_i^*(0) - \frac{i(\Delta\beta - 2\gamma W_1)}{2} A_s(0)}{\lambda} . \tag{89}$$

Substituting the results from (85) and (89) in (82) and, in turn, substituting in (80), we obtain the solution for the signal and idler as

$$A_s(z) = \left[A_s(0)\cosh\lambda z + \frac{i\gamma W_1 A_i^*(0) - \frac{i(\Delta\beta - 2\gamma W_1)}{2} A_s(0)}{\lambda} \sinh\lambda z \right] e^{\frac{i\Delta\beta z}{2}} e^{i\gamma W_1 z} =$$

$$= A_s(0)\left[\cosh\lambda z - \frac{i(\Delta\beta - 2\gamma W_1)}{2\lambda}\sinh\lambda z \right] e^{\frac{i\Delta\beta z}{2}} e^{i\gamma W_1 z} + A_i^*(0)\frac{i\gamma W}{\lambda}\sinh\lambda z\, e^{\frac{i\Delta\beta z}{2}} e^{i\gamma W_1 z} ,$$

$$A_i(z) = \left[A_i(0)\cosh\lambda z + \frac{i\gamma W_1 A_s^*(0) - \frac{i(\Delta\beta - 2\gamma W_1)}{2} A_i(0)}{\lambda} \sinh\lambda z \right] e^{\frac{i\Delta\beta z}{2}} e^{i\gamma W_1 z} =$$

$$= A_s^*(0)\frac{i\gamma W_1}{\lambda}\sinh\lambda z\, e^{\frac{i\Delta\beta z}{2}} e^{i\gamma W_1 z} + A_i(0)\left[\cosh\lambda z - \frac{i(\Delta\beta - 2\gamma W_1)}{2\lambda}\sinh\lambda z \right] e^{\frac{i\Delta\beta z}{2}} e^{i\gamma W_1 z} .$$

Same phase-sensitive behavior is also observed here. Phase of $A_i^*(0)$ term is given by $\frac{\pi}{2}-\theta$ and phase of $A_s(0)$ term is given by $\theta-\tan^{-1}\left(\frac{\Delta\beta-2\gamma W_1}{2\lambda}\tanh\lambda z\right)$. We have maximum amplification when both phases are equal, i.e. $\theta=\theta_{max}$ $=-\frac{\pi}{4}-\frac{1}{2}\tan^{-1}\left(\frac{\Delta\beta-2\gamma W_1}{2\lambda}\tanh\lambda z\right)$. We have phase-sensitive deamplification at $\theta=$ $\theta_{max}+\frac{\pi}{2}$.

Thus we have derived the solutions for nonlinearly coupled wave equations of parametric amplifier. We have shown that phase-sensitive amplification can be obtained in both phase-matched and phase-mismatched cases with either one or two pumps.

If only signal is present at the input, then the parametric amplifier operates in phase-insensitive regime. Indeed, the gain in that case is given by $G=\left|\frac{A_s(z)}{A_s(0)}\right|^2=\left|\cosh\lambda z-\frac{i(\Delta\beta-2\gamma W_1)}{2\lambda}\sinh\lambda z\right|^2=1+\left(\frac{\gamma W_1}{\lambda}\right)^2\sinh^2\lambda z$ and does not depend on θ. Figure 2.1 shows the phase-insensitive-amplification gain for degenerate pump case when the pump power W_1 varies from 0 to 1 Watt in the increments of 100 mW, dispersion D = +1 ps/nm/km at the pump wavelength λ_p=1550 nm, length of the fiber L = 1 km, and $\gamma=10$ $km^{-1}Watt^{-1}$ (typical for highly nonlinear fiber). The linear phase mismatch $\Delta\beta=-\beta''\omega_s^2$, where β'' and D are related as $D=-\frac{2\pi c}{\lambda_p^2}\beta''$. The phase-insensitive gain when the signal wavelength is 1550 nm is given by $G=1+(\gamma W_1 L)^2$.

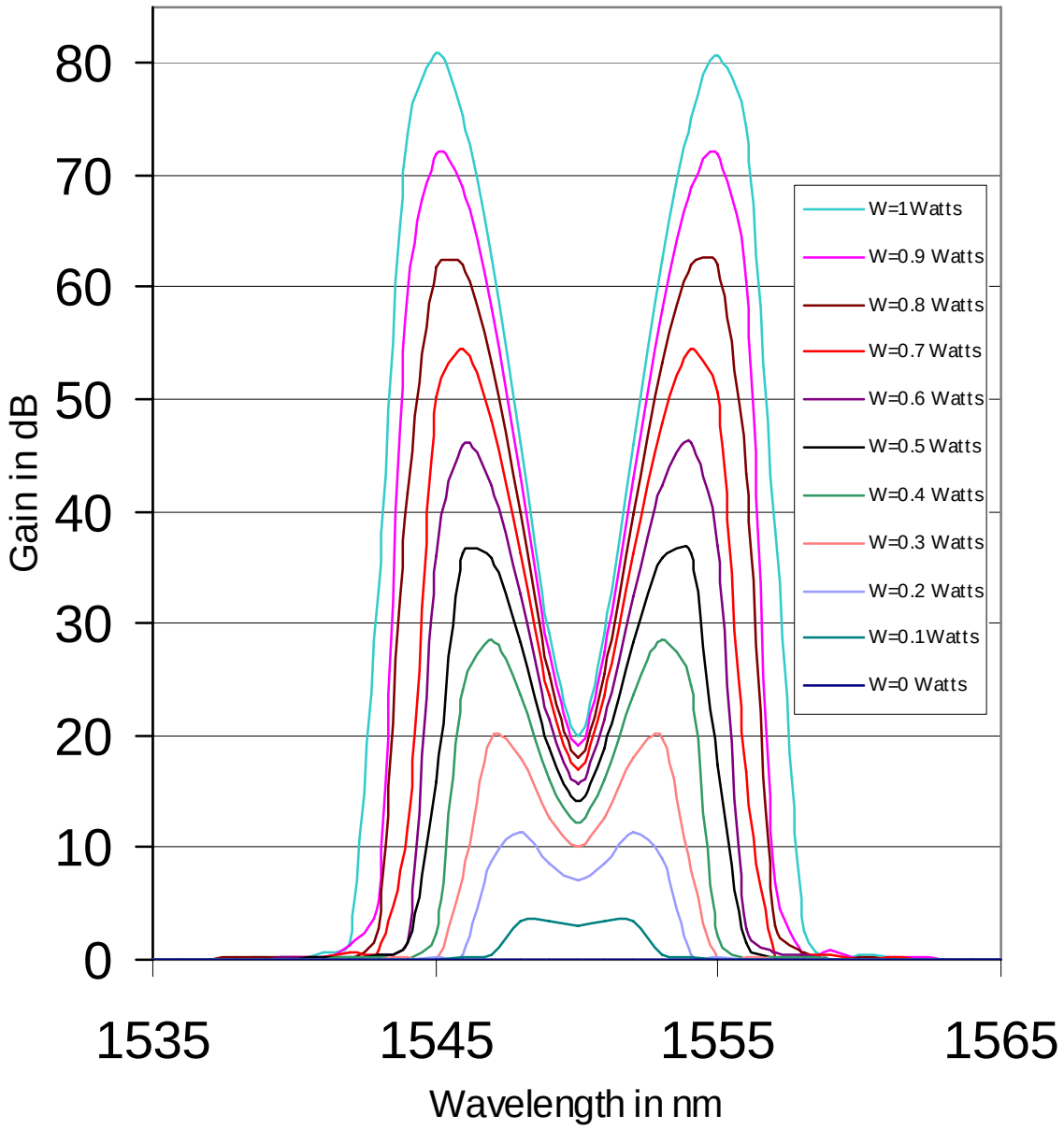

Figure 2.1. Phase-insensitive-amplification gain for degenerate pump case.

CHAPTER 3

DESIGN AND EXPERIMENTAL IMPLEMENTATION OF OPTICAL AMPLIFIER CONTROLS

3.1 Introduction

Parametric amplifiers and other nonlinear devices to be tested in our lab will be characterized by experimental recirculating-loop setup. While many of our devices are targeted for ultra-long-haul applications with transmission over dozens of fiber spans and thousands of kilometers, the cost and space considerations do not permit us to have more than several fiber spans in the lab. The recirculating loop allows characterization of the ultra-long-haul transmission performance with just a few spans of fiber by putting them in a loop and letting the signals circulate through it for many times before we take the measurements.

3.2 Experimental Setup

Figure 3.1 shows a schematic diagram of the experimental setup of recirculating loop to be built in our lab. 36 distributed feedback (DFB) lasers spaced by 100 GHz are multiplexed with an arrayed-waveguide grating (AWG) and modulated using a 10 Gb/s electro-optical modulator. To compensate for the losses of modulator and multiplexer we use an EDFA. The EDFA is followed by a variable optical attenuator and an acousto optic switch (AOS 1). The optical signal is fed into the recirculating loop via a 3-dB (50/50) coupler. In the recirculating loop we have 80 km of non-zero

dispersion shifted fiber (NZDSF) made by Corning Inc. (LEAF®), a variable optical attenuator and an acousto-optic switch (AOS 2). To compensate the dispersion of the NZDSF fiber, we use 2.5 km of dispersion-compensating fiber (DCF).

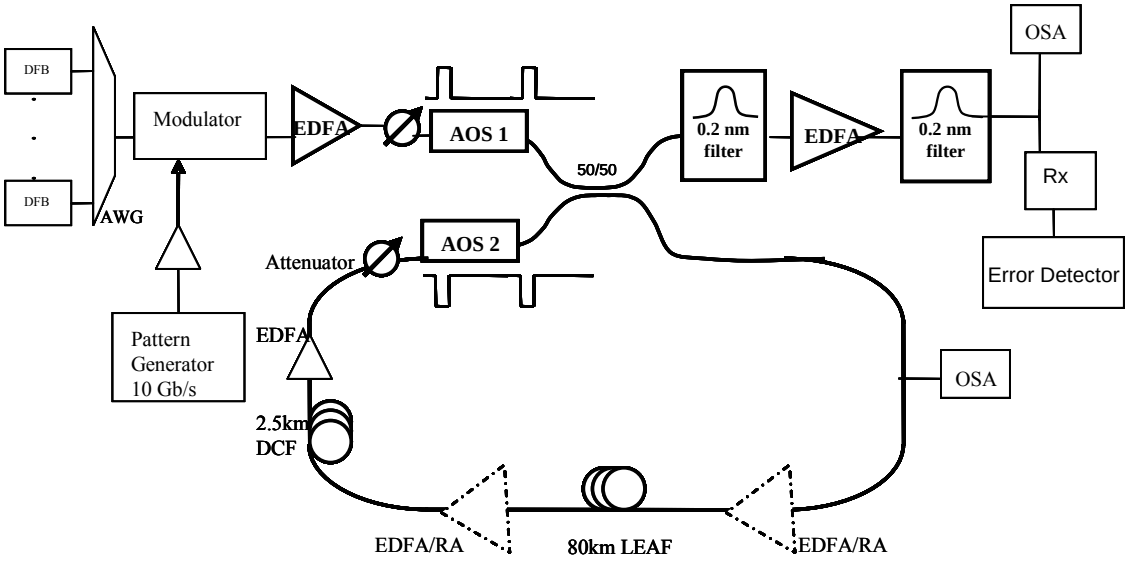

Figure 3.1. Experimental setup.

The acousto optic switches work in counter-phase: when first switch turns on, the second switch turns off, and vice versa. When AOS 1 is open, the signal goes into the 3-dB coupler and half of it goes into the recirculating loop. By the time the signal comes to the end of the loop, AOS 1 closes and AOS 2 opens. The signal circulates in the loop as long as AOS 2 is open. We can set the timing of the switches using a delay generator. The variable optical attenuator is designed to balance gain and loss after each round-trip so that the total signal powers after each round-trip are the same. This balance operation eliminates the wild transients of EDFAs that can damage the optical components in the loop.

We use 0.2-nm-wide optical band pass filter (OBPF) as a demultiplexer to select the channel to be measured. This channel is pre-amplified by an EDFA which is followed by another 0.2 nm OBPF which prevents the out-of-band spontaneous emission noise from entering the 10 Gb/s receiver Rx.

3.3 Erbium-doped fiber amplifiers

The erbium-doped fiber amplifier (EDFA) was first reported in 1987 [14, 15], and, in the short period since then, its applications have transformed the optical communication industry. The EDFA is an optical amplifier that faithfully amplifies lightwave signals purely in the optical domain. EDFAs have several functions in optical fiber transmission systems. They can be used as power amplifiers to boost transmitter power, as repeaters or in-line amplifiers to increase system reach, or as pre-amplifiers to enhance receiver sensitivity [16]. Optical amplifiers support the use of wavelength division multiplexing (WDM), whereby signals of different wavelengths are combined and transmitted together on the same transmission fiber. Erbium-doped fiber amplification is the key technology that enabled the deployment of multichannel WDM systems. In order to enable this growth in capacity the EDFAs have evolved to provide a higher performance and greater functionality.

In order to support the growth of channels in WDM transmission systems, optical amplifiers with wide bandwidth are required. The gain of amplifiers must be very uniform over the entire WDM transmission bandwidth for the channels to be transmitted without impairments due to either nonlinear effects in fiber or due to poor optical signal to noise ratio (OSNR) at the receiver. The power spectrum tilt in

wideband systems can arise from several reasons, such as EDFA gain tilt, spectral loss in transmission fiber, dispersion compensation fiber or other passive components, variation in input signal power due to uneven fiber span loss, and Raman effect.

In transmission system, the wide bandwidth of the amplifiers has to be maintained while accommodating the variations in the losses of fiber spans deployed in the field. The mid-stage attenuators provide control of the gain tilt of the amplifier over a wide range of variations in the span loss. This is achieved by maintaining the average inversion level of EDFA constant by changing the attenuator loss. The use of the attenuators, however, raises the concern about the increase of EDFA noise figure leading to the end–of–system OSNR degradation.

Optical amplifier gain is defined as the ratio of the output signal power to the input signal power,

$$G(\lambda) \equiv \frac{P_{\text{out}}}{P_{\text{in}}} = \int_0^L g(\lambda, z)\,\mathrm{d}z, \tag{90}$$

and is obtained by integrating the gain coefficient $g(\lambda)$ over the length L of the erbium-doped fiber. The gain coefficient, normally expressed in units of decibels per meter, is the sum of the emission coefficient $g^* = \Gamma_s n_{\text{Er}} \sigma_e(\lambda)$ and the absorption coefficient $\alpha(\lambda) = \Gamma_s n_{\text{Er}} \sigma_a(\lambda)$ weighed by the fractional populations N_2 and N_1, respectively, of the first excited and ground states of erbium:

$$g(\lambda, z) = \frac{1}{P(\lambda, z)} \frac{\mathrm{d}P(\lambda, z)}{\mathrm{d}z} = g^* N_2(z) - \alpha(z) N_1(z), \tag{91}$$

where n_{Er} is the maximum concentration of erbium ions in the core, Γ_s is the overlap integral of the signal mode and the erbium concentration profile, and $\sigma_e(\lambda)$ and $\sigma_a(\lambda)$ are, respectively, the emission and absorption cross sections as functions of wavelength.

The gain bandwidth of the EDFA extends from about 1525 to about 1600 nm, primarily as a result of the Stark splitting experienced by the high angular momentum ground and first excited states of the erbium ions in the local electric fields in the glass matrix. The gain spectrum, which is determined by the distribution of the Stark split sublevels and the thermal distribution of their populations, is not flat, and its shape changes with the level of inversion. Wysocki has shown that in an amplifier or in an amplified system the wavelength where the gain peaks can be predicted using average gain per unit length of the erbium-doped fiber to characterize the average inversion [17, 18]. It can be shown from (90) and (91) that the aggregate gain spectrum for an amplifier or system of amplifiers is given by the gain coefficient averaged over the length of erbium-doped fiber in the amplifier or system:

$$\overline{g}(\lambda) = g^*(\lambda)\,\overline{N}_2 - \alpha(\lambda)\,\overline{N}_1 = [g^*(\lambda) + \alpha(\lambda)]\overline{N}_2 + \alpha(\lambda) \quad ,$$

where the overbars indicate taking the average over the length of all the erbium-doped fiber in the amplifier system.

Figure 3.2 shows the gain coefficient as a function of average excited-state population $\overline{N}_2$ for a typical aluminum co-doped silica erbium-doped fiber. By setting $\overline{N}_2$ to zero and then one, we see that g^* and α are the gain and absorption per unit length of an EDFA in the limits of infinite and no pump, respectively. The intermediate

curves come from the uniparameter family of functions, which represent all gain spectra available from the erbium-doped fiber itself. Thus, $\overline{N}_2$ or closely related to it average inversion $\overline{N}_2 - \overline{N}_1$, impact the spectral shape of the EDFA's gain.

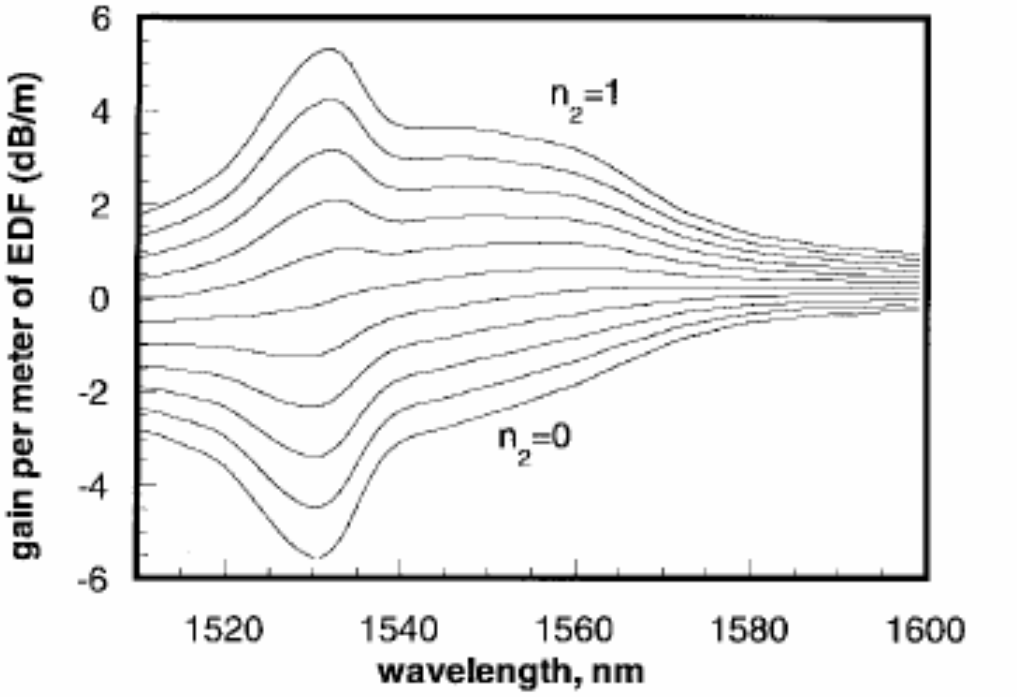

Figure 3.2. Gain per unit length of aluminum co-doped silica erbium doped fiber for relative excited-state population $\overline{N}_2$ ranging from 0 to 1.0 in increments of 0.1[19].

Let us discuss several key blocks of a modern EDFA.

Pre-amplifier Stage:

An optical preamplifier is designed primarily to achieve a low noise figure with about 20–30 dB of small-signal gain. This requires a low input coupling loss. A low-insertion-loss, high-isolation, polarization-independent isolator must be placed at the input to

prevent optical feedback from reflections that could result in lasing, with minimum degradation of the noise figure. It is also important to keep the average inversion level at the input as high as possible. This can be accomplished in a single stage amplifier by using a short segment of erbium-doped fiber and reverse pumping to minimize input coupling losses [16]. Multistage designs are not required to achieve these goals. However, in WDM systems requiring additional gain to compensate for the demultiplexer losses following the optical pre-amplifier, multistage pre-amplifier designs are generally used.

Optical pre-amplifiers are usually pumped at 980 nm because complete inversion is possible at this pumping wavelength. As long as the amplifier architecture allows sufficient 980 nm pump light near the input so that inversion is high there, quantum–limited noise figures approaching 3 dB are possible.

Power amplifier Stage:

A power amplifier is used to launch high-power signals to extend the transmission distance, or to permit splitting the signal. The erbium-doped fiber in a power amplifier is designed for the most efficient conversion of pump energy into signal energy [16]. In a single–stage amplifier, the length of the single erbium–doped fiber is made as long as possible so that the pump light is converted to signal energy as completely as possible. Additional pumps may be used to further increase the net output power. For amplifiers with two or more stages, interstage elements such as filters or isolators may be used to keep amplified spontaneous emission (ASE) from propagating and reducing the net inversion in the following or preceding stage. Pump reflectors,

which transmit the signal wavelengths, may be used to return into the gain medium unabsorbed pump light that would otherwise be lost.

Amplifiers using a hybrid of 1480 and 980 nm lasers have been designed with high output powers in the range of +20 dBm. The advantages of hybrid pumping over pumping at only 1480 nm include the suppression of pump crosstalk and the lowering of power consumption. The major drawback is the difficulty in providing pump redundancy.

Variable Optical Attenuator (VOA):

The gain tilt control is very important for the operation of WDM systems and networks. As we mentioned above, the variations in input signal power of EDFA will cause gain tilt at output. In addition, the spectrum of WDM channels after transmission through fiber can acquire positive (versus wavelength) linear tilt due to Raman effect which transfers power from shorter- to longer-wavelength channels [20]. It may be desirable to have a negative tilt in the spectrum of channels at the output of the amplifier in order to compensate for the Raman effect in the transmission fiber. Both of these conditions can be accommodated by controlling the gain tilt in the EDFA by a mid-stage VOA. This attenuator changes the power entering the power stage of EDFA which affects the inversion level and, therefore, the gain tilt. If the amount of VOA loss is significantly less than the pre-amplifier gain, then the net noise figure of two stage EDFA is largely determined by the pre-amplifier noise figure.

3.4 Operation of Erbium-doped fiber amplifiers

In our lab we are fortunate to have four EDFAs that were designed by Corning Inc. for Nortel (C+L)-band 160-channel Optera® system. The amplifiers we have are the high power (+18 dBm) L-band modules which operate in 1565–1605 nm region.

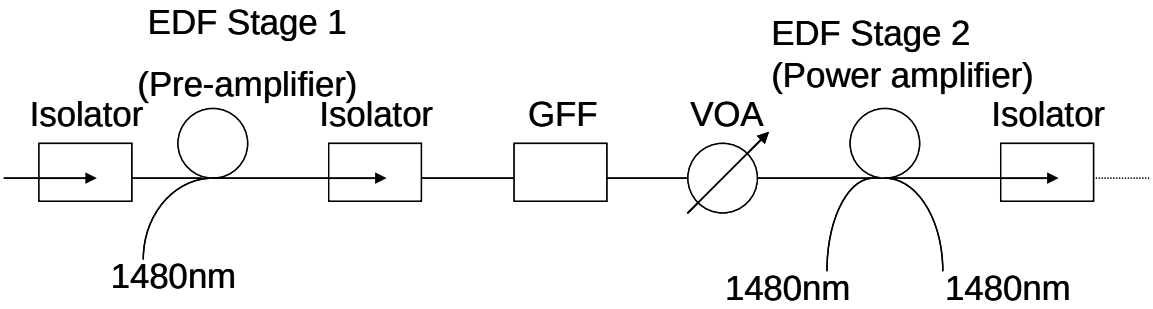

Figure 3.3. Schematic of two-stage EDFA.

Figure 3.3 shows the operational block diagram of our EDFA. The front stage (pre-amplifier) stage is in high-inversion regime and the power amplifier stage is in low inversion regime. The nominal signal power to our EDFA is +5 dBm and the output power is +18 dBm. The gain curve is flat for these conditions of operation. We have three pumps operating at 1480 nm, 1480 nm and 1480 nm respectively. The maximum pump current for pump1, pumps 2 and 3 is 650 mA. If the input power is less than +5 dBm then the amplifier works in high-inversion regime, and if the input power is greater than +5 dBm then the amplifier works in low-inversion regime. The pre-amplifier stage has approximately constant gain and power-amplifier stage has constant output power.

If the total average input power is +5 dBm, then the output power is +18 dBm, and the average gain of the system is 13 dB. If we increase the input power to +10 dBm,

the output power is still +18 dBm, therefore the overall gain is reduced to 8 dB, and amplifier is forced into lower-inversion regime causing positive gain tilt. In order to keep the gain curve flat, an extra attenuation is introduced by placing a VOA between pre-amplifier and power amplifier stages. If the signal power is less than +5 dBm then the amplifier is in high-inversion regime. We need to reduce the output power by adjusting the output pump currents so that the 13 dB gain is preserved, then the gain curve becomes flat. The noise figure is constant in the high-inversion regime (+5 dBm and lower input powers), but increases rapidly when higher signal power forces EDFA into a low-inversion regime.

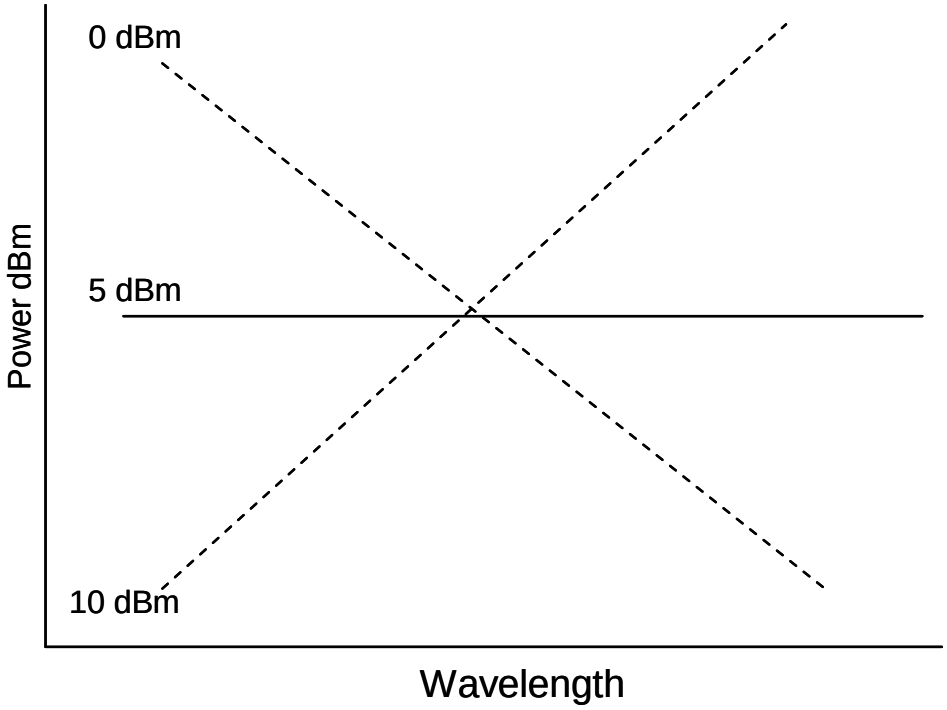

Figure 3.4. EDFA spectral tilt when the input signal power is 0 dBm, +5 dBm and +10 dBm.

3.5 Interface between EDFAs and our lab equipment

EDFAs that we have in our lab are supposed to be placed in Nortel rack which has a back plane with power supplies and laser diode drivers. Since we do not have Nortel rack, we need to build an interface between the EDFA and our lab equipment.

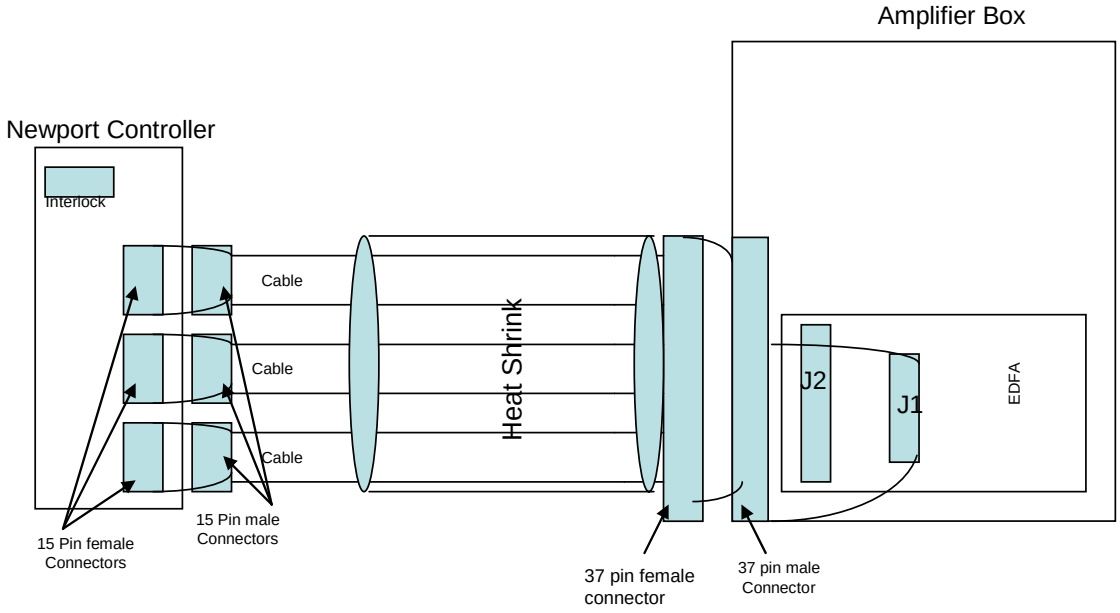

Figure 3.5. Schematic representing the connections between the amplifier and Newport controller 8016**.**

The Newport laser diode/ thermo-electric cooler (LD/TEC) controller 8016 has a 9-pin female interlock connector (pins 1 and 2 are shorted for laser diodes to operate) and sixteen plug-in boards (with 15-pin female connector on the back), each including laser diode driver and thermo-electric cooler controller. The 15-pin female connector on the Newport controller is connected to our home-made cable which on one end has three 15-pin male connectors and on the other end has a 37-pin female connector. We

designed the cable interface between Newport controller and EDFA as shown in Figure 3.5. The picture of the cable is shown in Figure 3.6.

Figure 3.6. Cable interface between Newport 8016 LD/TEC controller and EDFAs.

The EDFA has a 50-pin connector for LD/TEC control and a 70- pin connector for VOA control.

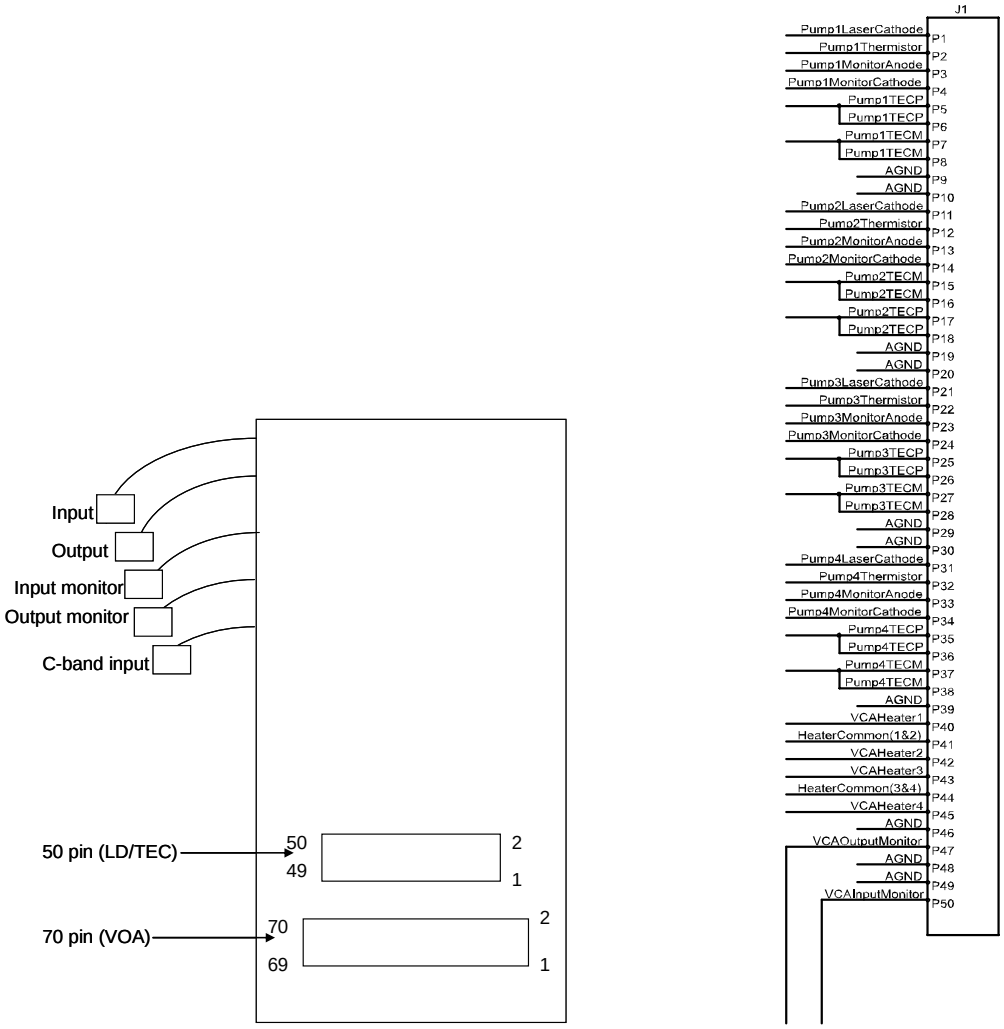

Figure 3.7. Schematic showing the layout of the EDFA and pin configuration of 50-pin connector on the EDFA.

The 37-pin female connector on our home-made cable is connected to the 37-pin male connector on the back of the amplifier box. EDFAs are fixed to the base of the box. The EDFA has a 50-pin connector (J1) and a 70-pin connector (J2). The other end of the 37- pin male connector on the amplifier box is in turn connected to J1 on the EDFA. J2 on the EDFA is connected to the Variable Optical Attenuator (VOA) and is discussed in next section.

The amplifier is fixed on the bottom of the amplifier box which on the front face has push buttons that control the variable optical attenuator and on the back face has two 37-pin male connectors connected to the cable interface as shown in Figure 3.8.

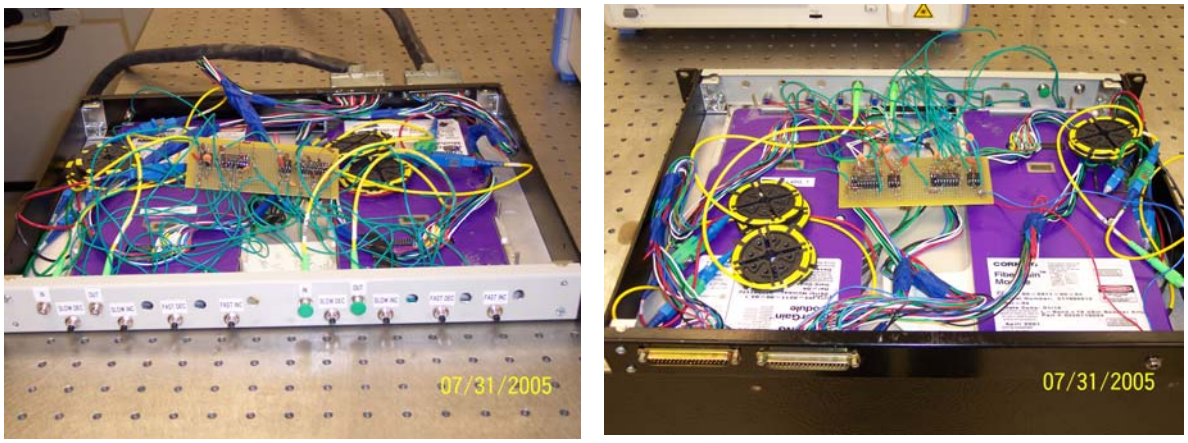

Figure 3.8. Front and back faces of the amplifier box.

The pin connections between pump1, pump2, pump3 and the 37-pin connector are shown in Figures 3.9, 3.10 and 3.11, respectively.

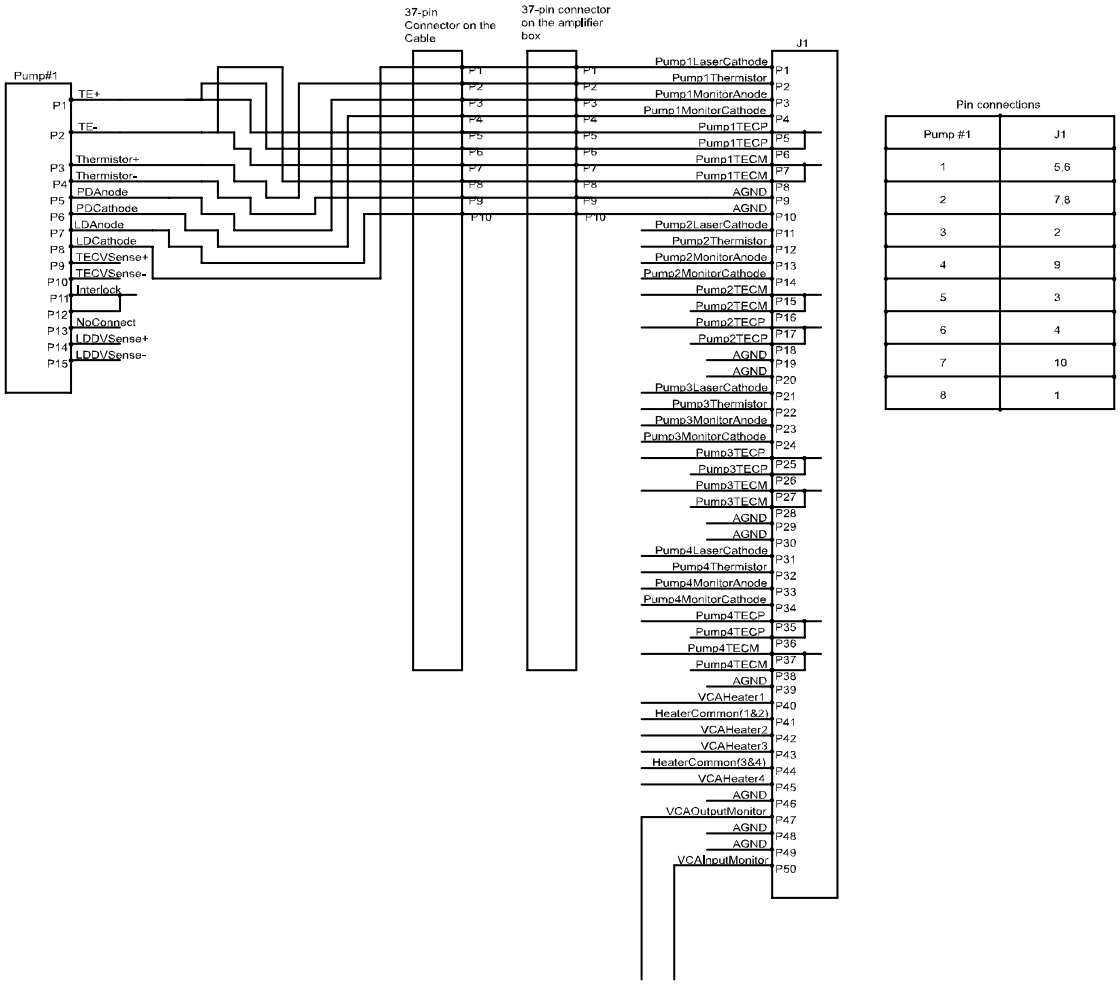

Pin connections

Pump #1	J1
1	5,6
2	7,8
3	2
4	9
5	3
6	4
7	10
8	1

Figure 3.9. Pin connections between pump 1 and 50-pin connector on the amplifier.

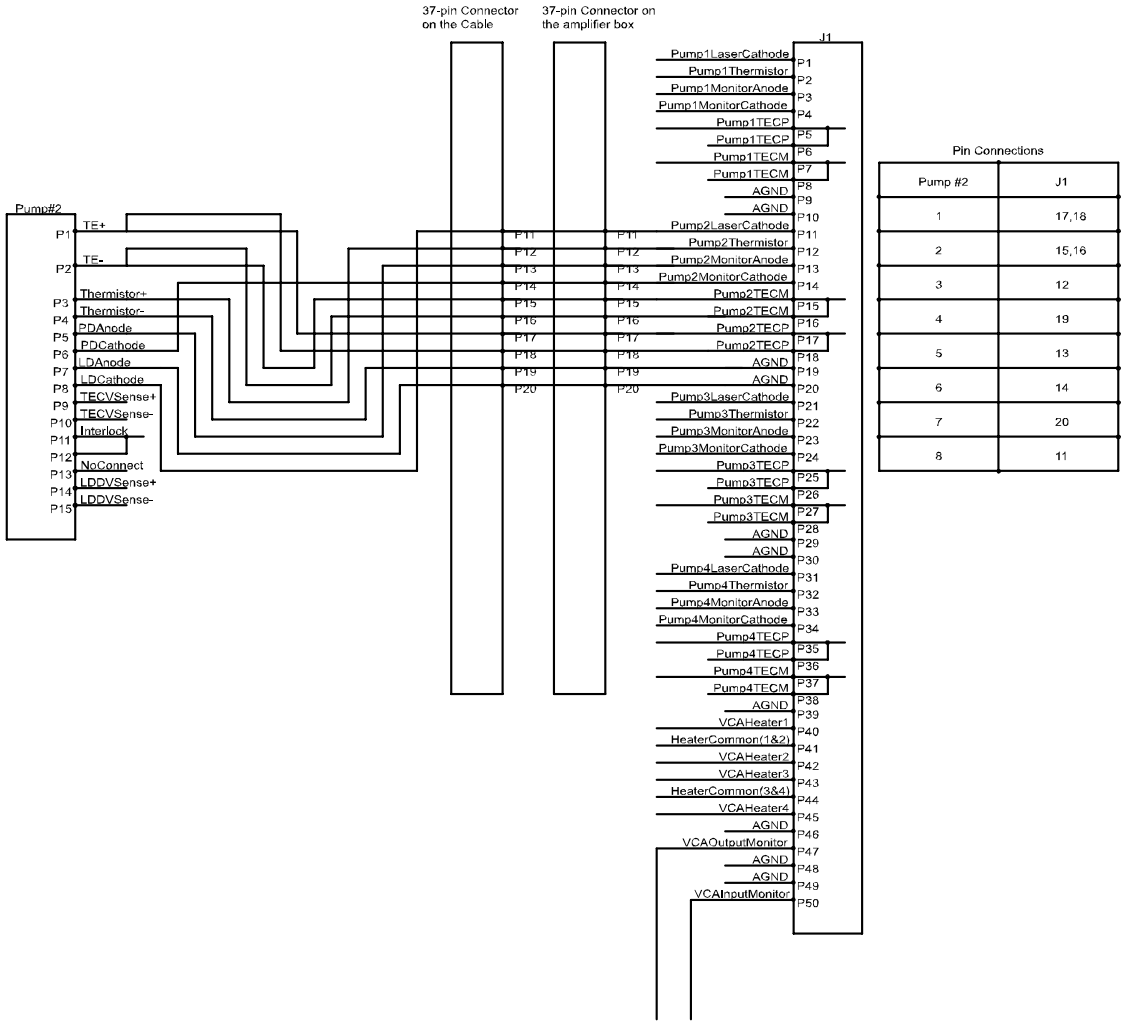

Figure 3.10. Pin connections between pump 2 and 50-pin connector on the amplifier.

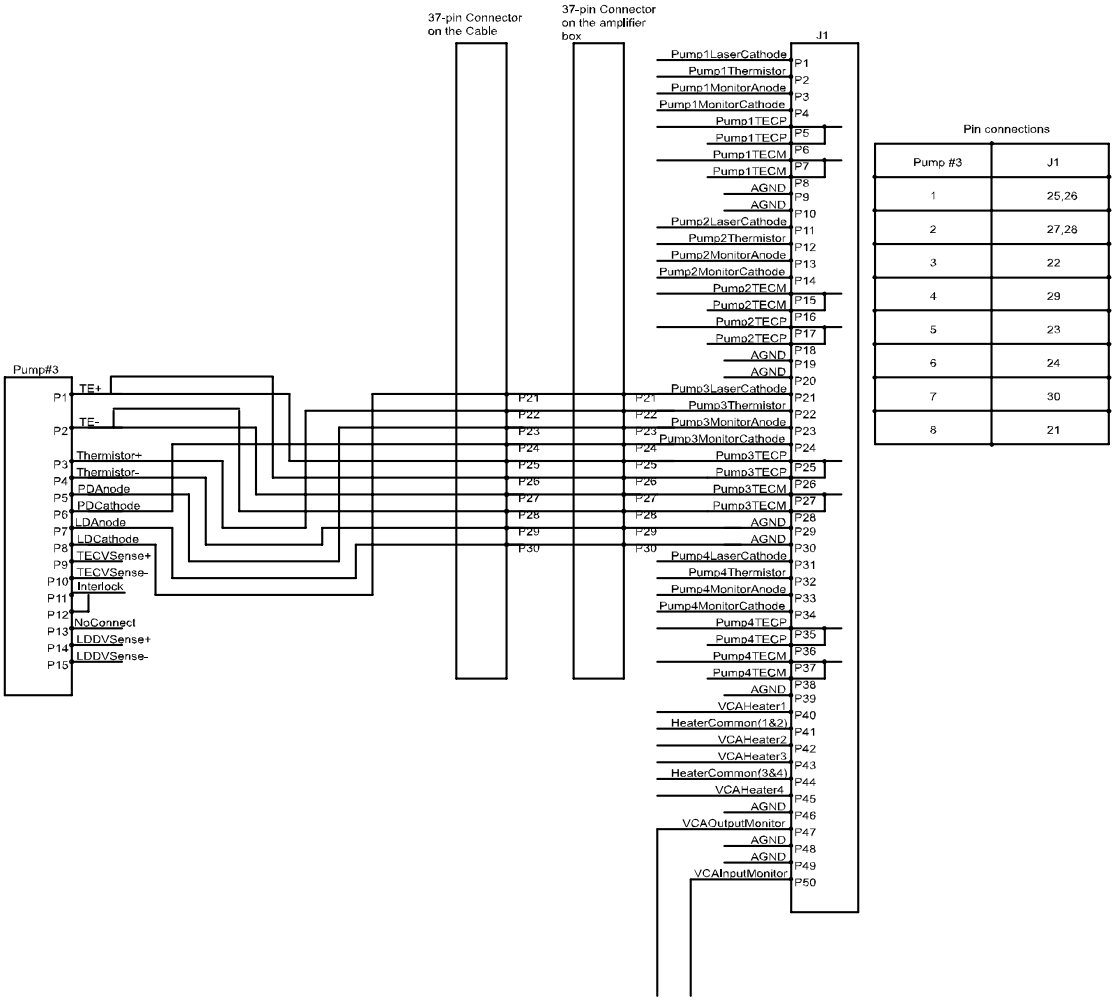

Figure 3.11. Pin connections between pump 3 and 50-pin connector on the amplifier.

How to turn on the pumps:

After connection, check that all TECs are reporting room temperature correctly, i.e. ~23C and not -8.3C or +353C or something odd. Then switch on the TECs one at a time, checking that each TEC is controlled to its set point (25^{o}C). After all the TECs are successfully controlled you can switch on the laser diodes, in the order from pump 1, pump 2, pump 3. The pumps should be turned off in the backward order (the pump turned on last should be turned off first).

The 1480-nm diodes should not be driven above 650 mA

Table 3.1. 15-Pin Connector Pinouts.

Pin	Description	
1	TE+	Can be two wires each
2	TE-	
3	Thermistor +	
4	Thermistor-	
5	PD Anode	
6	PD Cathode	
7	LD Anode	
8	LD Cathode	
9	TEC V Sense +	Not Used
10	TEC V Sense-	
11	Interlock	Shorted inside Cable's 15-pin connector
12	Interlock (GND)	
13	No Connect	
14	LDD V Sense+	Not Used
15	LDD V Sense-	

Table 3.2. List of hardware purchased for cable interface.

Stock Number/Description Mouser	Price	Stock Number/Description Allied Electronics	Price
523-17D-15P MFG PN: 17 -DA15P 15P PLUG SOLDER CUP Amphenol D-Subminiature Connectors	$2.10	216-3727 MFG PN: 9751 CHROME CX/100 BELDEN WIRE AND CABLE CABLE	$92.18
523-17-1657-15 MFG PN: 17 -1657-15 D-SUB HOOD CAST ZINC Amphenol D-Subminiature Connectors	$3.05	618-3927 MFG PN: 151250 -8322-TB 3M/INTERCONNECT SOLUTIONS 50 pin Connector	$6.10
523-17D-C375 MFG PN: 17 -DC37S 37P RECPT SOLDER CUP Amphenol D-Subminiature Connectors	$8.17	708-7251 MFG PIN: FIT221 ¾ 4` BLACK BX/5 ALPHA WIRE Heat Shrink	$12.25
523-17D-C37P MFG PN: 17 -DC37P 37P PLUG SOLDER CUP Amphenol D-Subminiature Connectors	$5.83		
523-1731657-37 MFG PN: 17 -1657-37 D-SUB COMM ACC Amphenol D-Subminiature Connectors	$5.16		

3.6 Variable Optical Attenuator

The Nortel amplifier has VOA inside driven by a stepper motor controlled by TTL control voltages. To provide this control functionality, we have built the circuit shown in Figure 3.12.

The controller inputs for the VOA are INCrement and DECrement.

- INC: The INCrement input is used to increment the stepper motor within the VOA assembly. INCrementing the stepper motor means to INCrease the attenuation. For each high to low logic transition applied to the INCrement input, the stepper motor will rotate one step in the CW (clockwise) direction. The maximum INCrement step rate is limited to 488 Hz. The minimum pulse width must be $\geq$256 μs [either in a high (logic “1”) or low (logic “0”) state].

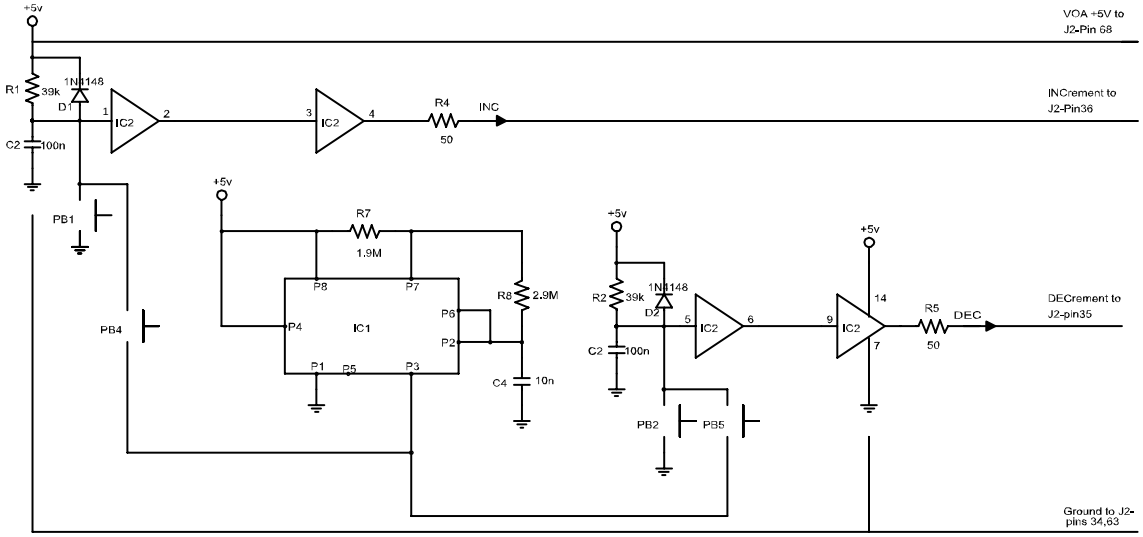

Figure 3.12 Variable Optical Attenuator circuit.

- DEC: The DECrement input is used to decrement the stepper motor within the VOA assembly. DECrementing the stepper motor means to DECrease the attenuation. For each high to low logic transition applied to the DECrement input, the stepper motor will rotate one step in the CCW (counterclockwise) direction. The maximum DECrement step rate is limited to 488 Hz. The minimum pulse width must be $\geq 256\ \mu s$ [either in a high (logic "1") or low (logic "0") state].
- VOA +5V/GND: The input voltage range is $+4.57 \leq V_{cc} \leq +5.25$ Volts. Positive +5V DC is connected to VOA +5V pin 68 of J2 on the amplifier. The GND is pin 34 or 63 of J2 (34 and 63 are connected on the amplifier board). J2 refers to the amplifier's 70-pin connector.

Table 3.3. Components required for building the VOA circuit.

Designation	Part Description
R1	39kΩ
R2	39kΩ
R4	50Ω
R5	50Ω
R7	1.9MΩ
R8	2.9MΩ
C1	.1μf
C2	.1μf
C4	.01μf
D1	1N4148
D2	1N4148
PB1	Signal Increase
PB2	Signal Decrease
PB4	Steady Increase
PB5	Steady Decrease
IC1	555 Timer 8pin
IC2	74HC14 14pin Schmidt Trigger
Power Supply	+5Vdc, 600mA.

All Push Buttons are momentary and normally opened These buttons must be low bounce.

The pin configuration of 70-pin connector to which the VOA circuit is connected is shown in Figure 3.13.

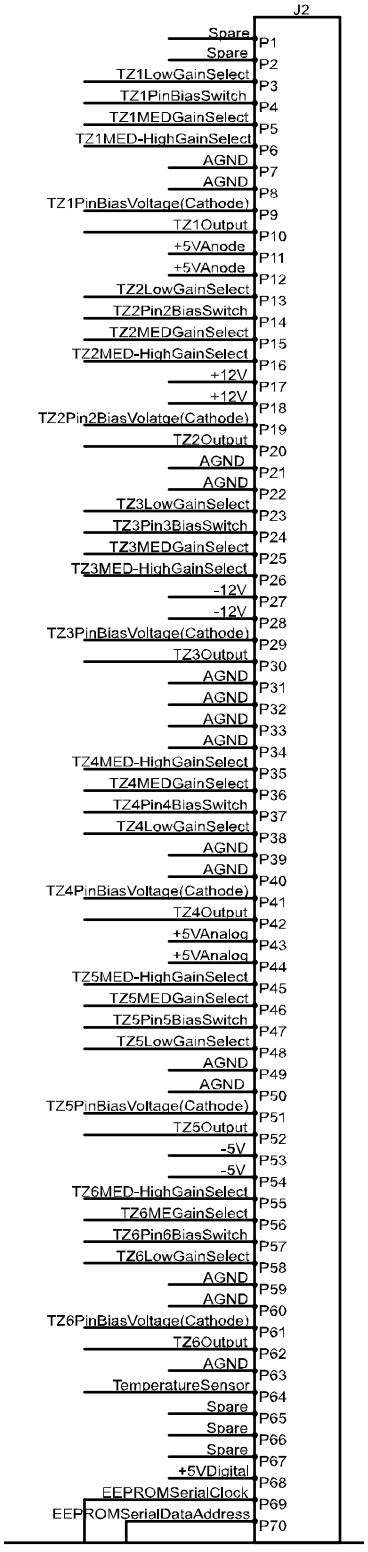

Figure 3.13. Pin configuration of the 70-pin connector on the EDFA.

3.7 Experimental Results

To demonstrate the operation of the designed interface and the circuit board a series of measurements have been performed. The first measurement demonstrates the dependence of the gain tilt on the value of mid-stage attenuation. When the variable optical attenuator is fully open, we have minimum attenuation, and when the VOA is closed, we have maximum attenuation. We utilize an input signal from tunable laser to saturate the amplifier, and use the output amplified spontaneous emission spectrum as an indicator of the gain shape.

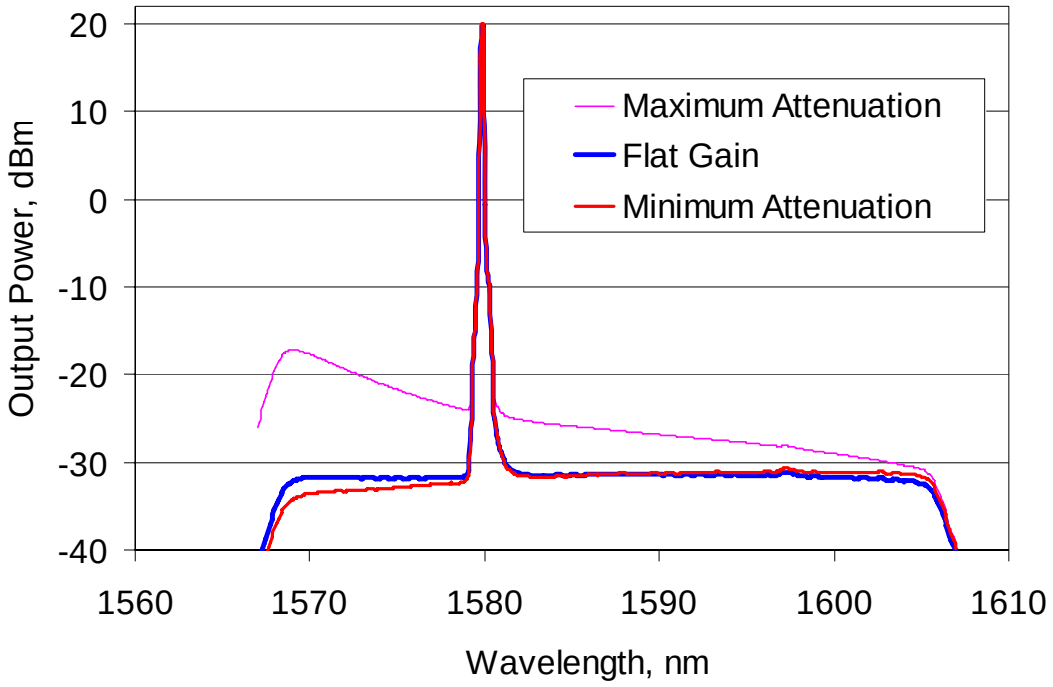

Figure 3.14. Output responses when the VOA is fully closed, partially opened, and fully open.

Figure 3.14 shows the EDFA output spectrum curves for maximum attenuation, minimum attenuation and flat-gain response when the input signal power is +7 dBm, and the pump currents are 200 mA, 500 mA and 500 mA for pumps 1, 2, and 3,

respectively. One can see that, for +7 dBm input power, finite VOA attenuation is needed in order to compensate the positive tilt and achieve flat gain.

The next set of measurements deals with the dependence of gain on input power. Figure 3.15 shows the output spectra when the input power is +4.5 dBm, +7 dBm, and 0 dBm; VOA is completely open and the pump currents are 250 mA, 600 mA and 600 mA for pumps 1, 2 and 3, respectively. One can easily see that the change from negative (high inversion) to positive (low inversion) tilt as the input power increases from 0 to +7 dBm.

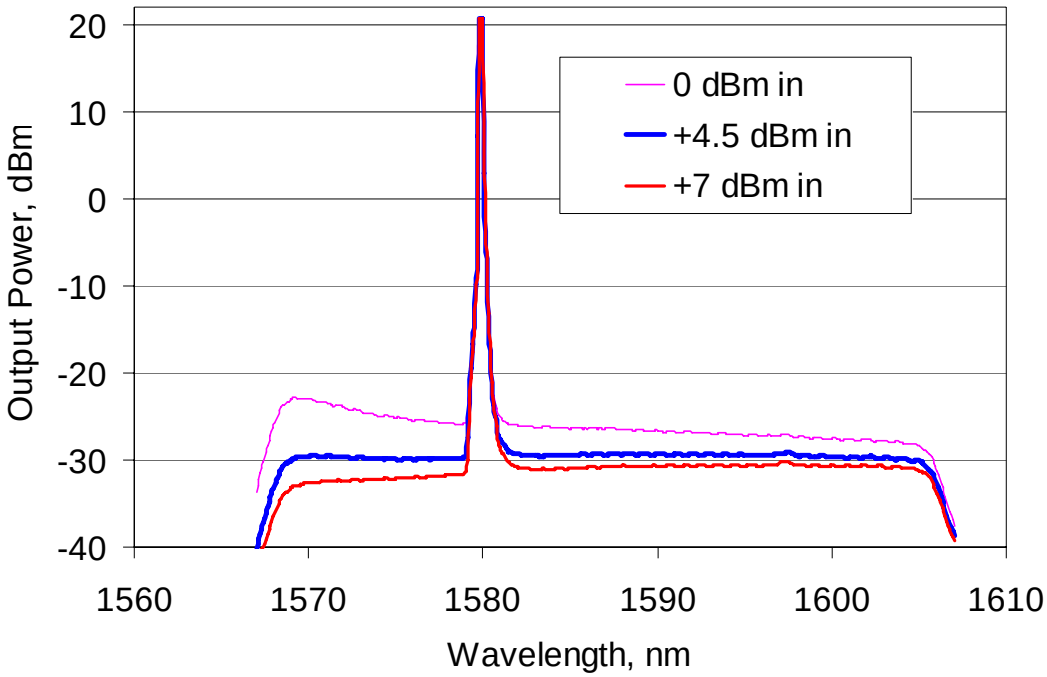

Figure 3.15. Output response when the input signal power is 0 dBm, +4.5 dBm, and +7 dBm; VOA is fully opened, and the pump currents are 250 mA, 600 mA, and 600 mA.

In our amplifier, the flat response was obtained at +4.5 dBm input power which is slightly different from the nominal power for flat spectrum. A flat response can be

produced at +5 dBm input power by increasing the pump currents to 650 mA, 650 mA and 650 mA on pumps 1, 2 and 3, respectively.

The dependence of the gain tilt on VOA attenuation and input power level, demonstrated by Figures 3.14 and 3.15, is in line with our expectations described in Section 3.4. Therefore, we can conclude that our interface and control circuitry are working properly.

CHAPTER 4

CONCLUSIONS

This work is focused on laying down a better foundation for testing of parametric amplifiers and other nonlinear devices in our lab.

We have derived the equations of parametric amplification in optical fiber and found their solutions when signal, idler and pump beams are linearly co-polarized. We have considered both non-degenerate and degenerate pump cases with arbitrary phase mismatch and proved that the amplifier can perform phase-sensitive amplification in both cases.

We have also designed an experimental recirculating-loop setup for testing all the nonlinear devices to be used in our lab, an interface between telecom-industry EDFAs and the laser diode drivers and thermo electric coolers used in our lab, and a control circuit for variable optical attenuator (VOA) which enables the amplifier to operate at various input power levels.

We have also performed a series of measurements that demonstrate the flawless operation of the designed interface and VOA circuit board.

Future work

The optical amplifiers designed in this work are the key components of recirculating-loop testbed described in chapter 3.2. The recirculating-loop testbed will be used to test the parametric amplifiers and other nonlinear-optical devices.

REFERENCES

[1] M. Vasilyev, "Raman-assisted transmission: toward ideal distributed amplification," invited paper WB1 at *Optical Fiber Communication Conference 2003*.

[2] A. F. Evans, A. Kobyakov, and M. Vasilyev, "Distributed Raman transmission: applications and fiber issues," book chapter in *Raman amplifiers and oscillators in telecommunications*, ed. by M. N. Islam, Springer-Verlag, to come out in 2003.

[3] M. Vasilyev, B. Szalabofka, S. Tsuda, J. M. Grochocinski, and A. F. Evans, "Reduction of Raman MPI and noise figure in dispersion-managed fiber," Electron. Lett. **38**, 271 (2002).

[4] J.-C. Bouteiller, K. Brar, and C. Headley, "Quasi-constant signal power transmission," *European Conference on Optical Communication 2002*, paper S3.04.

[5] E. E. Narimanov and P. Mitra, "The channel capacity of a fiber optics communication system: perturbation theory," J. Lightwave Technol. **20**, 530 (2002).

[6] C. M. Caves, "Quantum limits on noise in linear amplifiers," Phys. Rev. D. **26**, 1817 (1982).

[7] D. Levandovsky, M. Vasilyev, and P. Kumar, "Amplitude squeezing of light by means of a phase-sensitive fiber parametric amplifier," Opt. Lett. **24**, 984 (1999).

[8] D. Levandovsky, M. Vasilyev, and P. Kumar, "Near-noiseless amplification of light by a phase-sensitive fiber amplifier," PRAMANA–Journal of Physics **56**, 281 (2001).

[9] J. A. Levenson, I. Abram, T. Rivera, and P. Grainger, "Reduction of quantum-noise in optical parametric amplification," J. Opt. Soc. Am. B **10**, 2233 (1993).

[10] Z. Y. Ou, S. F. Pereira, H. J. Kimble, "Quantum noise reduction in optical amplification," Phys. Rev. Lett. **70**, 3239 (1993).

[11] S.-K. Choi, M. Vasilyev, and P. Kumar, "Noiseless Optical Amplification of Images," Phys. Rev. Lett. **83**, 1938 (1999).

[12] M. Vasilyev, "Disributed phase-sensitive amplification," submitted to Opt. Express.

[13] S. Radic, C. J. McKinstrie, "Two pump fiber parametric amplifiers," Opt. Fiber Technol. **9**, 7 (2003).

[14] E. Desurvire, J.R Simpson and P. C. Becker. "High-gain erbium-doped fiber amplifier," Opt. Lett. **12**:888 (1987).

[15] R.J. Mears, L. Rekkie, I.M. Jauncey, and D.N. Payne, "Low-noise erbium-doped fiber amplifier operating at 1.54 μm.," Electronic Lett. **23** (1987).

[16] I P. Kaminow, T L. Koch, "*Optical fiber telecommunications, Volume IIIB*," Academic Press, chapter 2 (1997).

[17] P.F. Wysocki, J.R Simpson and D. Lee, "Prediction of gain peak wavelength for Er-doped fiber amplifiers and amplifier chains," IEEE Photon. Tech. Lett. **6** (1994).

[18] P.F. Wysocki, J.R Simpson and D. Lee, "Simple theory of gain peaking in erbium-doped amolifier chains for long-haul communications in Fiber laser sources and amplifiers" *V,* ed. M. J. Digonnet, 146. SPIE Proceedings No. 2073. Bellingham, WA: SPIE. (1994).

[19] M.J. Yadlowsky, E.M Deliso, and V.L Dasilva, "Optical Fiber Amplifiers for WDM Systems," Proc. IEEE **85**, No. 11 (1997).

[20] I P. Kaminow, T Li, "*Optical fiber telecommunications Volume IVA*," Academic Press, Chapter 4 (2002).

BIOGRAPHICAL INFORMATION

Sravanthi Thotakura was born on 24th of June, 1982 in Vijayawada, Andhra Pradesh, India. She completed her school and pre-university education in Vijayawada, Andhra Pradesh in 1999. She received Bachelor of Technology from Jawaharlal Nehru Technological University, Hyderabad, Andhra Pradesh in April 2003. Since August 2003 she is working towards Masters Degree in Electrical Engineering at University of Texas at Arlington.